THE JOURNAL OF BIOLOGICAL CHEMISTRY VOL. 290, NO. 8, pp. 4908–4927, February 20, 2015

Phosphorylation of Synaptic GTPase-activating Protein (synGAP) by Ca^{2+}/Calmodulin-dependent Protein Kinase II (CaMKII) and Cyclin-dependent Kinase 5 (CDK5) Alters the Ratio of Its GAP Activity toward Ras and Rap GTPases*[S]

Received for publication, September 25, 2014, and in revised form, December 17, 2014 Published, JBC Papers in Press, December 22, 2014, DOI 10.1074/jbc.M114.614420

Ward G. Walkup IV[‡1], Lorraine Washburn[‡], Michael J. Sweredoski[§], Holly J. Carlisle[‡2], Robert L. Graham[§3], Sonja Hess[§], and Mary B. Kennedy[‡4]

From the [‡]Division of Biology and Biological Engineering, and the [§]Proteome Exploration Laboratory of the Beckman Institute, California Institute of Technology, Pasadena, California 91125

Background: synGAP inactivates Ras and Rap at synapses.
Results: Phosphorylation of synGAP by CaMKII increases Rap1 GAP activity more than HRas GAP activity; phosphorylation by CDK5 has the opposite effect.
Conclusion: Phosphorylation by CaMKII and CDK5 alters the ratio of Rap1 and HRas GAP activities.
Significance: Phosphorylation of synGAP by CaMKII and CDK5 can alter the balance of synaptic functions regulated by Ras and Rap.

synGAP is a neuron-specific Ras and Rap GTPase-activating protein (GAP) found in high concentrations in the postsynaptic density (PSD) fraction from the mammalian forebrain. We have previously shown that, *in situ* in the PSD fraction or in recombinant form in Sf9 cell membranes, synGAP is phosphorylated by Ca^{2+}/calmodulin-dependent protein kinase II (CaMKII), another prominent component of the PSD. Here, we show that recombinant synGAP (r-synGAP), lacking 102 residues at the N terminus, can be purified in soluble form and is phosphorylated by cyclin-dependent kinase 5 (CDK5) as well as by CaMKII. Phosphorylation of r-synGAP by CaMKII increases its HRas GAP activity by 25% and its Rap1 GAP activity by 76%. Conversely, phosphorylation by CDK5 increases r-synGAP's HRas GAP activity by 98% and its Rap1 GAP activity by 20%. Thus, phosphorylation by both kinases increases synGAP activity; CaMKII shifts the relative GAP activity toward inactivation of Rap1, and CDK5 shifts the relative activity toward inactivation of HRas. GAP activity toward Rap2 is not altered by phosphorylation by either kinase. CDK5 phosphorylates synGAP primarily at two sites, Ser-773 and Ser-802. Phosphorylation at Ser-773 inhibits r-synGAP activity, and phosphorylation at Ser-802 increases it. However, the net effect of concurrent phosphorylation of both sites, Ser-773 and Ser-802, is an increase in GAP activity. synGAP is phosphorylated at Ser-773 and Ser-802 in the PSD fraction, and its phosphorylation by CDK5 and CaMKII is differentially regulated by activation of NMDA-type glutamate receptors in cultured neurons.

The PSD[5] contains cytosolic signaling complexes associated with glutamate receptors at the postsynaptic membrane of excitatory synapses. synGAP, a dual Ras and Rap GAP, is abundant in the PSD of excitatory synapses (1, 2). The family of small GTPases, including Ras and Rap, act as effectors of a wide variety of signaling proteins, including several located in neuronal synapses and dendrites (3). They adopt an active conformation when bound to GTP and are inactivated when they hydrolyze the bound GTP to GDP. GAP proteins, including synGAP, increase the rate of inactivation of small GTPases by binding to them and accelerating the rate at which GTP is hydrolyzed.

The GAP domain of synGAP is homologous to that of p120GAP and neurofibromin, two canonical rasGAPs that do not regulate Rap (1, 2, 4). Nevertheless, synGAP has been shown to stimulate the GTPase activity of Rap about 100 times more potently than that of Ras (5, 6). Pena *et al.* (6) found that the upstream C2 domain of synGAP works with the GAP domain to enable acceleration of Rap GTPase activity. synGAP is the only example of a RapGAP that requires a second domain in addition to the GAP domain for its catalytic activity.

* This work was supported, in whole or in part, by National Institutes of Health Grant MH095095 (to M. B. K.). This work was also supported by grants from the Gordon and Betty Moore Foundation (Center for Integrative Study of Cell Regulation), the Hicks Foundation for Alzheimer's Research, and the Allen and Lenabelle Davis Foundation.
[S] This article contains supplemental material.
[1] Supported by National Institutes of Health Grant 5 T32 GM07616 from NRSA and National Science Foundation Graduate Research Fellowship Grant 2006019582.
[2] Present address: Dept. of Neuroscience, Amgen, Thousand Oaks, CA 91360.
[3] Present address: Institute of Cancer Sciences, Faculty of Medical and Human Sciences, University of Manchester, Manchester M13 9PL, United Kingdom.
[4] To whom correspondence should be addressed: Division of Biology and Biological Engineering 216-76, California Institute of Technology, Pasadena, CA 91125. Tel.: 626-395-3924; Fax: 626-395-8474; E-mail: kennedym@its.caltech.edu.

[5] The abbreviations used are: PSD, postsynaptic density; CaMKII, Ca^{2+}/calmodulin-dependent protein kinase II; CDK5, cyclin-dependent kinase 5; GAP, GTPase-activating protein; LB, lysogeny broth; PDZ, PSD-95, Discs-large, ZO1; SEC, size exclusion chromatography; synGAP, synaptic GTPase-activating protein; r-synGAP, soluble active recombinant synGAP fragment comprising residues 103–1293; sr-synGAP, soluble active recombinant synGAP fragment comprising residues 103–725; TCEP, tris(2-carboxyethyl)phosphine; CsA, cyclosporin A; NMDAR, NMDA receptor; AMPAR, AMPA receptor; BisTris, 2-[bis(2-hydroxyethyl)amino]-2-(hydroxymethyl)propane-1,3-diol; CaN, calcineurin; OKA, okadaic acid; ANOVA, analysis of variance; Ab, antibody.

synGAP is tightly associated with the postsynaptic plasma membrane and binds to the PSD-95, Discs-large, ZO1 (PDZ) domains of PSD-95 (1, 2), which positions it in close proximity to the NMDA-type and AMPA-type glutamate receptors (NMDARs and AMPARs), respectively. Loss of one copy of the synGAP gene produces cognitive dysfunction in mice (7) and humans (8), indicating that the functions of synGAP are critically important for normal synaptic regulation. Influx of Ca^{2+} through NMDARs and binding of ligands to TrkB (BDNF/neurotrophin-3 growth factors receptor B) receptors can activate Ras and Rap postsynaptically (3, 9, 10). Over time, Ras and Rap modulate synaptic strength in opposite directions. Active Ras increases insertion (exocytosis) of AMPARs at the synapse, whereas active Rap increases their removal (endocytosis) from the synapse (10). Here, we investigated whether phosphorylation of individual residues on synGAP could alter the ratio of its Ras and Rap GAP activities such that the balance of these two activities, and thus the balance of active Ras and Rap, could be changed under different physiological conditions.

We previously showed that activation of NMDARs on cultured CNS neurons leads to phosphorylation of synGAP by CaMKII (1, 9, 11), and we identified several major sites on partially purified, membrane-bound synGAP where phosphorylation by CaMKII increases its Ras GAP activity (11). Here we show, with purified and soluble recombinant synGAP lacking the first 102 N-terminal residues (r-synGAP), that phosphorylation by CaMKII increases its HRas and Rap1 GAP activities by 25 and 76%, respectively, but does not affect its Rap2 GAP activity.

We also show that r-synGAP is a substrate for CDK5, which phosphorylates it at two sites, Ser-773/Thr-775 and Ser-802. CDK5 is a proline-directed serine/threonine kinase that is involved in many neuronal processes, including regulation of synaptic plasticity (12–14). It is localized at synapses and interacts with or regulates synaptic proteins, including NR2A (15), PSD-95 (16), and CaMKII (17).

We found that phosphorylation of r-synGAP by CDK5 increases its HRas and Rap1 GAP activities by 98 and 20%, respectively. Thus, phosphorylation of synGAP by CaMKII accelerates the rate of inactivation of Rap1 more potently than the rate of inactivation of HRas, whereas phosphorylation by CDK5 has the opposite effect. We show that Ser-773 and Ser-802 are both phosphorylated in a mouse PSD fraction. Furthermore, phosphorylation by the two kinases is dynamically regulated by NMDA receptors in cultured neurons. These results mean that differential phosphorylation of synGAP by CaMKII and CDK5 may alter the proportions of activated Ras and Rap in synapses with consequent effects on cellular processes regulated by the two GTPases.

EXPERIMENTAL PROCEDURES

Cloning, Expression, and Purification of r-synGAP—Soluble recombinant synGAP comprising residues 103–1293 (r-synGAP) was purified from *Escherichia coli*. Pena *et al.* (6) had previously shown that removal of the N-terminal 102 residues and several hundred residues from the C terminus enabled purification of a soluble active fragment of synGAP comprising residues 103–725 (sr-synGAP). Gene fragments encoding rat r-synGAP and sr-synGAP (AF048976) were amplified by PCR with PfuUltra II fusion HS (Agilent, catalog no. 600670) and cloned by the polymerase incomplete primer extension-ligation-independent cloning method (18, 19) into pET-47b(+) (EMD Millipore, catalog no. 71461) in-frame with an N-terminal His_6 tag and a PreScission protease cleavage site. The DNA sequence was verified by Sanger sequencing (Laragen). The plasmids were transformed into the Rosetta2(DE3) *E. coli* strain (EMD Millipore, catalog no. 71397) for protein expression. Single colonies were grown overnight at 37 °C in 5 ml of Miller lysogeny broth (LB; EMD Millipore, catalog no. 71753-6) supplemented with 50 μg/ml kanamycin and 34 μg/ml chloramphenicol. Cultures grown overnight were diluted 1:500 into LB and grown at 37 °C for 4–6 h to an A_{600} of 1.0. Cultures were then chilled to 18 °C, and protein expression was induced with 0.2 mM isopropyl 1-thio-β-D-galactopyranoside for 24 h. Bacterial pellets were harvested by centrifugation and resuspended in Lysis/Wash Buffer (20 mM Tris, 500 mM NaCl, 10 mM tris(2-carboxyethyl)phosphine (TCEP; Gold Biotechnology, catalog no. TCEP25), 5 mM $MgCl_2$, 60 mM imidazole, 2 mM ATP, 1 mM PMSF (Sigma, catalog no. P76726), 0.2% Tergitol^{TM}-type Nonidet P-40, and Complete EDTA-free protease inhibitor (Roche Applied Science, catalog no. 5056489001), pH 7.0) supplemented with 25 units/ml benzonase (EMD Millipore, catalog no. 71206) and 10 kilounits/ml ReadyLyse (Epicenter, catalog no. R1810M). Cells were lysed with an ML-110 microfluidizer (Microfluidics), and insoluble material was removed by centrifugation at 30,000 × *g*. r-synGAP in the supernatant was bound to 1.5 ml of Talon metal affinity resin per g of cell pellet (Clontech, catalog no. 635503) by batch absorption for 90 min. The resin was poured into a gravity-fed column and washed with 10 column volumes of Lysis/Wash Buffer. r-synGAP was eluted with Lysis/Wash Buffer (−2 mM ATP) supplemented with 10 mM EDTA and 250 mM imidazole. Fractions containing synGAP were pooled and concentrated by ultrafiltration through a 150-kDa cutoff filter (Thermo Scientific, catalog no. 89923) for r-synGAP, and a 9-kDa cutoff filter (Thermo Scientific, catalog no. 89885A) for sr-synGAP. The presence of 0.2% Tergitol^{TM} was necessary to prevent loss of synGAP on the filter. Concentrated samples of r-synGAP (0.25–1 mg/ml) were then exchanged into Storage Buffer by ultrafiltration (20 mM Tris, 500 mM NaCl, 10 mM TCEP, 5 mM $MgCl_2$, 1 mM PMSF, 0.2% Tergitol^{TM}-type Nonidet P-40, and Complete EDTA-free protease inhibitor, pH 7.0), flash-frozen in liquid nitrogen, and stored at −80 °C. Concentrated samples of sr-synGAP were further purified on a HiLoad 26/600 Superdex 200 preparation grade column (GE Healthcare, catalog no. 28-9893-36) equilibrated with Storage Buffer. Fractions containing sr-synGAP were pooled, concentrated by ultrafiltration to 2 mg/ml, flash-frozen in liquid nitrogen, and stored at −80 °C. All mutant forms of r-synGAP were purified by the same procedure as for wild type r-synGAP.

Cloning, Expression, and Purification of HRas, Rap1, and Rap2—Gene fragments coding for full-length rat HRas (AAA42009.1), human Rap1B (CAB46488), and human Rap2A (CAA31052.1) were amplified by PCR and inserted into pGEX-6P-1 expression vectors (GE Healthcare, catalog no. 28-9546-48) at a site bound by EcoRI and XhoI recognition sites and

in-frame with an N-terminal GST tag and a PreScission Protease cleavage site. The sequence of each plasmid was verified, and they were transformed into Rosetta2 *E. coli* cells (EMD Millipore, catalog no. 71402-4) for protein expression. Single colonies were grown overnight at 37 °C in 5 ml of LB supplemented with 100 μg/ml carbenicillin and 34 μg/ml chloramphenicol. Overnight cultures were diluted 1:500 into LB supplemented with 2% glucose and grown at 37 °C for ~4–6 h to an A_{600} of 1.0. Cultures were then chilled to 22 °C, and protein expression was induced with 0.1 mM isopropyl 1-thio-β-D-galactopyranoside for 4 h. Bacterial pellets were harvested by centrifugation, resuspended in GTPase Lysis/Wash Buffer (50 mM Tris, 100 mM NaCl, 5 mM TCEP, 5 mM $MgCl_2$, 1 mM EDTA, 1 mM PMSF, 30 μM GDP, 0.1% Triton X-100, Complete protease inhibitor, pH 7.5) supplemented with 25 units/ml benzonase, and 10 kilounits/ml ReadyLyse, and lysed by fluidization. Insoluble material was removed by centrifugation at 30,000 × *g*. The expressed protein in the supernatant was bound to 0.3 ml of glutathione-agarose resin per g of cell pellet (Thermo Scientific, catalog no. 16100) by batch absorption for 3 h. The resin was poured into a gravity-fed column and washed with 20 column volumes GTPase Lysis/Wash Buffer. GTPases were eluted with Cleavage Buffer (50 mM Tris, 100 mM NaCl, 5 mM TCEP, 5 mM $MgCl_2$, 1 mM EDTA, 30 μM GDP, 0.1% Triton X-100, and 50 mM glutathione, pH 8.0). Fractions containing the GTPases were pooled and concentrated by ultrafiltration through a 9-kDa cutoff filter. Concentrated samples of GTPase were mixed with 20 units/ml PreScission Protease (GE Healthcare, catalog no. 27-0843-01) and cleaved for 18 h at 4 °C to release GST. Samples were exchanged into SEC Buffer (20 mM Tris, 100 mM NaCl, 5 mM TCEP, 5 mM $MgCl_2$, 1 mM PMSF, 30 μM GDP, and 10% glycerol, pH 8.0) and concentrated by ultrafiltration before being fractionated on a HiLoad 26/600 Superdex 75 preparation grade column (GE Healthcare, catalog no. 28-9893-33) equilibrated with SEC buffer. Fractions containing GTPases were pooled, concentrated by ultrafiltration to greater than 1 mg/ml, flash-frozen in liquid nitrogen, and stored at −80 °C. After SEC, all three GTPases were purified to >95% purity, with yields of ~25%. The intrinsic k_{cat} values of purified GTPases, measured in our assay, were 0.0008, 0.0001, and 0.00008 s^{-1}, for HRas, Rap1, and Rap2, respectively.

SDS-PAGE and Assessment of Protein Purity and Yield—We used SDS-PAGE to determine the purity of proteins and to quantify yields throughout the purification process. Protein samples were diluted 1:4 into 4× LDS buffer (catalog no. NP0007) and heated to 70 °C for 10 min before fractionation on NuPAGE Novex 4–12% BisTris SDS-polyacrylamide gradient gels (catalog no. NP0336PK2) run under reducing conditions with NuPAGE antioxidant (catalog no. NP0005) and MOPS running buffer (catalog no. NP0001–02), all purchased from Life Technologies. Proteins were stained with Gel Code Blue (Thermo Scientific, catalog no. 24592), imaged on a Li-Cor Odyssey Classic Infrared Imaging System (Li-Cor Biosciences) at 700 nm, and quantified with LiCor Image Studio Software (version 4.0.21) against standard curves of bovine serum albumin (BSA, catalog no. A7517-1VL), lysozyme (catalog no. L4631-1VL), or LacZ (catalog no. G8511-1VL), all purchased from Sigma. The protein standards were loaded onto each gel in lanes adjacent to the protein samples. Molecular weights of stained proteins were verified by comparison with Precision Plus Protein All Blue Standards (Bio-Rad, catalog no. 161-0373).

Site-directed Mutagenesis of CDK5 Phosphorylation Sites in r-synGAP—Ten r-synGAP mutants were prepared to study the effects of specific CDK5 phosphorylation sites on synGAP activity. They included single mutations S773A, T775A, S802A, S773D, T775D, and S802D; double mutations S773A/T775A, S773D/T775D, and S773D/S802D; and the triple mutation S773A/T775A/S802A. Oligonucleotides encoding these mutations were designed with the QuikChange II primer design program (Agilent) and were synthesized by Integrated DNA Technologies (IDT). Mutations of synGAP were made with the QuikChange II XL site-directed mutagenesis kit (Agilent, catalog no. 200522).

Site-directed Mutagenesis of CaMKII Phosphorylation Sites in r-synGAP—A mutant r-synGAP (CTM-Plus) was constructed based on the CTM-mutant, published earlier (11), by adding mutations of newly identified CaMKII phosphorylation sites to determine their effects on synGAP activity. Serine and threonine residues at sites 750, 751, 756, 764, 765, 1058, 1062, 1064, 1093, 1095, 1099, 1123, and 1125 in synGAP were all replaced with alanine residues. A pair of complementary oligonucleotides encoding serine to alanine mutations of 750, 751, 756, 764, and 765 was designed with DNA2.0 Gene Designer (version 1.1.4) (DNA2.0) and IDT Oligo Analyzer software and synthesized by IDT. Mutagenesis of r-synGAP was performed with a QuikChange II XL site-directed mutagenesis kit, as described previously (20), to generate the CTM-half. Next, a pair of large oligonucleotides encoding mutations to alanine at sites 1058, 1062, 1064, 1093, 1095, 1099, 1123, and 1125 was designed and synthesized as described above. The second oligonucleotide pair was inserted into the CTM-half cDNA by the polymerase incomplete primer extension-ligation-independent cloning method (18, 19) to generate the CTM-Plus cDNA. CTM-Plus was transformed into One-shot TOP10 chemically competent cells (Life Technologies, catalog no. C4040-06) for propagation, and the DNA sequence was verified.

Stoichiometry and Rate of r-synGAP Phosphorylation by CaMKII and CDK5—Phosphorylation of r-synGAP by CaMKII (purified as described in Ref. 21) or by CDK5/p35 (EMD Millipore, catalog no. 14-477M) was carried out in a 250-μl reaction mixture containing 50 mM Tris-HCl, pH 8.0, 10 mM $MgCl_2$, 0 (CDK5) or 0.7 mM (CaMKII) $CaCl_2$, 0.4 mM EGTA, 30 or 500 μM (as indicated) [γ-^{32}P]ATP (100–375 cpm/pmol), 0 (CDK5) or 3.375 μM (CaMKII) calmodulin, 10 mM DTT, 286 nM r-synGAP, and 3.1 nM rat brain CaMKII or 110 nM CDK5/p35. Carrier-free γ-labeled ATP (6000 Ci/mmol, PerkinElmer Life Sciences, catalog no. BLU002Z/NEG002Z) was diluted to the desired specific activity by addition of unlabeled ATP (Sigma, catalog no. A2383-25G). Phosphorylation was initiated by addition of ATP to a reaction mixture prewarmed to 30 °C. At the indicated time points, reaction aliquots were removed and quenched by the addition of 0.25 volume of ice-cold 4× LDS Sample Buffer containing 10% β-mercaptoethanol. Samples were fractionated by SDS-PAGE as described above. Gels were rinsed in water, wrapped in Saran Wrap, and exposed to a Stor-

age Phosphor screen (GE Healthcare, catalog no. 63-0034-79) for 2–4 h to locate phosphorylated proteins. To quantify the amount of phosphate incorporated, the density of ^{32}P bands was determined by scanning with a Typhoon LA 9000 PhosphorImager (GE Healthcare) followed by analysis with ImageQuant TL software (GE Healthcare, catalog no. 29000737). Relative densities were converted to picomoles of phosphate by comparison with densities from standard amounts of [γ-^{32}P]ATP spotted onto filter paper and imaged simultaneously. The stoichiometry of phosphorylation was calculated by dividing the picomoles of incorporated phosphate by the amount of synGAP (3.8 pmol) loaded per lane.

Confirmation of r-synGAP Phosphorylation by CaMKII or CDK5/p35 by Western Blotting—For Western blotting, phosphorylation of r-synGAP was carried out, as described above, except with 30 or 500 μM cold ATP in place of [γ-^{32}P]ATP. After SDS-PAGE, proteins were electrically transferred to PVDF membranes (Thermo Scientific, catalog no. 8520) in 25 mM Tris, 200 mM glycine, and 20% methanol. Membranes were washed with 50 mM Tris-HCl, 150 mM NaCl, pH 7.6 (TBS), followed by blocking with Odyssey Blocking Buffer (Li-Cor Biosciences, catalog no. 927-40003). Membranes were washed in TBS supplemented with 0.1% Tween before incubation in Odyssey Blocking Buffer or 5% Fraction V BSA (Sigma, catalog no. A9418-100G) in TBS (phosphosite antibodies only) containing one or more of the following dilutions of primary antibodies: 1:2000 mouse anti-bovine serum albumin (Abcam, catalog no. ab3781, RRID, AB_304073); 1:2000 rabbit anti-phospho-synGAP-Ser-1123 (MBK Laboratory; see Ref. 11); 1:2000 rabbit anti-phospho-synGAP-Ser-764/5 (MBK Laboratory; see Ref. 11); 1:1000 rabbit anti-synGAP (Thermo Scientific, catalog no. PA1-046, RRID, AB_2287112); 1:500 rabbit anti-pSer CDK substrate (Cell Signaling Technology, catalog no. 2324S, RRID, AB_2244779 (discontinued, replacement catalog no. 9477)); and 1:1000 mouse BSA-free anti-Tetra-His (Qiagen, catalog no. 34670). Bound antibodies were detected with 1:10,000 donkey anti-rabbit IRdye700 (Rockland Immunochemicals, catalog no. 610-731-124, RRID, AB_220145) or goat anti-rabbit IRdye800 (Rockland Immunochemicals, catalog no. 611-132-002, RRID, AB_1660971), or 1:10,000 goat anti-mouse Alexa-Fluor 680 (Life Technologies, catalog no. A21057, RRID, AB _10562421), visualized with a Li-Cor Odyssey Classic Infrared Imaging System and quantified with the Li-Cor Image Studio software (version 4.0.21).

GTPase Assays—The GTPases were loaded with [γ-^{32}P]GTP by nucleotide exchange as described previously (15, 22, 23). HRas, Rap1, or Rap2 (200 μM) were first incubated in 25 mM Tris, pH 8.0, 100 mM NaCl, 5 mM DTT, 15 mM EDTA, 100 mM NH_4SO_4, and 10 mM GTP for 60 min at room temperature. The exchange reactions were terminated by the addition of 25 mM $MgCl_2$. GTPases were concentrated and separated from unbound nucleotides and EDTA by ultrafiltration at 4 °C in an Amicon concentrator (EMD Millipore, catalog no. UFC501096). GTPases were then loaded with [γ-^{32}P]GTP by incubating GTP-bound GTPase (0.8 or 1.6 mM) with 10 μCi of [γ-^{32}P]GTP (6000 Ci/mmol; PerkinElmer Life Sciences, catalog no. BLU004Z/NEG004Z) in the presence of 12 mM EDTA for 40 min on ice. The exchange reaction was terminated by addition of 25 mM $MgCl_2$. [γ-^{32}P]GTP-bound HRas or Rap GTPases were diluted to the desired concentration before use in GTPase assays.

The GTPases pre-loaded in this way undergo one round of hydrolysis of the bound GTP at fixed, slow intrinsic rates as follows: $\sim 4-8 \times 10^{-4}\ s^{-1}$ (Ras) and $\sim 0.5-1 \times 10^{-4}\ s^{-1}$ (Rap1 and -2). When synGAP is added to an assay under these conditions, it acts as a catalyst, accelerating the rate of the single hydrolysis reactions. The acceleration of hydrolysis of GTP by HRas, Rap1, or Rap2 by synGAP was assayed by measuring the rate of release of [γ-^{32}P]phosphate as described previously (24). Briefly, phosphorylated or nonphosphorylated synGAP (250–500 nM) was mixed with increasing concentrations of each GTPase bound to radioactive [γ-^{32}P]GTP at 25 °C in 6.5 μl of Assay Buffer (25 mM Tris, pH 8.0, 100 mM NaCl, 15 mM $MgCl_2$, and 5 mM DTT) as described previously (15). After 10 min, the assay was quenched with activated charcoal in phosphate buffer to adsorb proteins GTP and GDP. Following removal of the charcoal, free [γ-^{32}P]phosphate was quantified by scintillation counting in Beta Blend scintillant (MP Biomedicals, catalog no. 0188245001). Initial rates of GTP hydrolysis for each concentration of GTPase with and without synGAP were determined after fitting the data by linear regression. The rates were plotted against the corresponding concentrations of GTPase with Prism software (version 6.0d, GraphPad Software, La Jolla, CA), and the data were fit to a hyperbolic curve by nonlinear regression. The Michaelis-Menten equation was used to calculate k_{cat} and K_m values.

Phosphorylation of r-synGAP by CaMKII or CDK5/p35 for Use in GAP Assays—Phosphorylation of synGAP by CaMKII or CDK5/p35 was carried out immediately prior to GAP assays in reaction mixtures containing 50 mM Tris-HCl, pH 8.0, 10 mM $MgCl_2$, 0 (CDK5) or 0.7 mM (CaMKII) $CaCl_2$, 0.4 mM EGTA, 30 μM ATP, 0 (CDK5), or 3.375 μM (CaMKII) calmodulin, 10 mM DTT, 725 nM r-synGAP, and 10 nM rat brain CaMKII or 230 nM CDK5/p35. Phosphorylation was initiated by addition of ATP to reaction mixtures prewarmed to 30 °C. At the indicated time points, aliquots were removed from the reaction and quenched by the addition of ⅓ volume of ice-cold Kinase Quench Buffer (20 mM Tris-HCl, pH 8.0, 396 mM NaCl, 2 mM DTT, 30 mM EGTA, 0.2% Tergitol^{TM}-type Nonidet P-40, 90 μM roscovitine (Sigma, catalog no. R7772-5MG) and 6 μM auto-camtide 2-related inhibitory peptide (Sigma, catalog no. A4308)). Samples were stored on ice until their addition to GAP assays.

Mass Spectrometry of Phosphorylated r-synGAP—Mass spectrometry of r-synGAP was performed by the Proteome Exploration Laboratory at the California Institute of Technology. r-synGAP was phosphorylated for 2 and 10 min in the presence of 30 μM ATP as described above, except with unlabeled ATP. All liquid chromatography-mass spectrometry (LC-MS) experiments were performed on an EASY-nLC (Proxeon Biosystems, now Thermo Scientific) connected to a hybrid LTQ-FT (Thermo Scientific) equipped with a nano-electrospray ion source (Proxeon Biosystems, now Thermo Scientific) essentially as described previously (25), with the modifications indicated below. Peptides were separated on a 15-cm reverse phase analytical column (75 μm inner diameter) packed in-house with 3 μm ReproSil-Pur C18AQ beads (Dr. Maisch GmbH,

catalog no. r13.aq.) with a 60-min gradient at a flow rate of 350 nl/min. The gradient was run from 0 to 40% solvent B (97.8% acetonitrile, 0.2% formic acid, 2% water) in 40 min, increased to 100% B in 1 min, and run at 100% B for 19 min. The mass spectrometer was operated in data-dependent mode to automatically switch between full scan MS and MS2 acquisition. Survey full scan mass spectra were acquired in ion cyclotron resonance, over a range of 400–1800 m/z, following accumulation of 1,000,000 ions, with a resolution of 100,000 at 400 m/z. The top five most intense ions from each survey scan were isolated and, after the accumulation of 5000 ions, fragmented in the linear ion trap by collision-induced dissociation (collisional energy 35% and isolation width 2 Da). Additionally, an MS3 neutral loss scan was acquired to detect loss of phosphoric acid (32.67, 49.00, or 97.97 m/z) in the top five most intense peaks in the MS2. Precursor ion charge state screening was enabled, and all singly charged and unassigned charge states were rejected. The dynamic exclusion list was set with a maximum retention time of 90 s and a relative mass window of 10 ppm, and early expiration was enabled.

Tandem mass spectra were converted to mgf files with the use of ReAdW4Mascot2 (peptide.nist.gov/metrics). MS3 spectra were separated from MS2 spectra, and accurate masses were determined for MS3 precursor spectra by the method of Timm *et al.* (26). All MS/MS samples were analyzed with the use of Mascot (version 2.2.06, MatrixScience). We constructed a sequence database containing the sequence of synGAP and common contaminants, including keratins and trypsin (262 entries). Trypsin was specified as the digestion enzyme, and up to two missed cleavages were allowed. We set mass tolerances of 10 ppm for parent ions and 0.50 Da for fragment ions. Carbamidomethylation of cysteine (+57.0215 Da) was specified in Mascot as a fixed modification, and oxidation of methionine (+15.9949 Da), dehydration of serine and threonine (−18.0106 Da, only MS3 spectra), and phosphorylation of serine, threonine, and tyrosine (+79.9663 Da, only MS2 spectra) were specified as variable modifications. Mascot results were loaded into Scaffold (version 3.00.06, Proteome software) and filtered at a protein probability of 99% with a minimum of two peptides and a peptide probability of 95%. We calculated false localization rates of phosphorylation sites using the Mascot Delta-score as described by Savitski *et al.* (27). In this algorithm, peptides with only one possible phosphorylation site are given a false localization rate of zero. Summaries of data and annotated spectra for all phosphorylation sites are included in the supplemental material.

Detection of Phosphorylated Ser-773 and Ser-802 in the PSD Fraction by Mass Spectrometry—Aliquots of PSD fraction from mice (65–125 μg), prepared as described below, were incubated with 0 or 30 μM ATP for 10 min in 120 μl of the reaction mix described above. In some experiments, exogenous CDK5/p35 (1–2 units) and/or 100 μM roscovitine (Sigma, catalog no. R7772-5MG) were added. Proteins were fractionated by SDS-PAGE and stained with Gel Code Blue, and the 140–160-kDa bands containing synGAP were excised and digested with trypsin in the gel as described previously (28). synGAP samples were analyzed on an Orbitrap Fusion (Thermo Scientific) equipped with a nano-electrospray ion source coupled to an EASY-nLC. Peptides were separated on a 25-cm reverse phase analytical column (75 μm inner diameter) packed in-house with 3 μm ReproSil-Pur C18AQ beads with a 100-min gradient at a flow rate of 350 nl/min. The gradient ran from 2% solvent B (80% acetonitrile, 0.2% formic acid, 19.8% water) to 40% solvent B in 90 min, then increased to 100% in 1 min, and held at 100% for 9 min. A parallel reaction-monitoring strategy (29) was employed to monitor the levels of phosphorylation on synGAP at sites Ser-773 and Ser-802. Precursor ions were isolated in the quadrupole, fragmented by HCD, and sent to the Orbitrap measurement (isolation width 1 Da, normalized collision energy of 35%, AGC target of 100,000 ions with a maximum injection time of 50 ms). The peptides monitored for phosphorylation at site Ser-773 included LPSPTK (m/z 361.6779, $z = 2$), GLNSSMDMARLPSPTK (m/z 595.6072, $z = 3$), GLNSSMDMARLPSPTK (m/z 606.2705, $z = 3$), and LPSPTKEKPPPPPPGGGK (m/z 620.9922, $z = 3$). The peptide monitored for phosphorylation at site Ser-802 was SSPAYCTSSSDITEPEQK (m/z 1033.9166, $z = 2$). Special caution was taken to identify the correct chromatographic peak based on fragment ions unique to phosphorylation at Ser-802 and not Tyr-805, Thr-807, Ser-808, Ser-809, or Ser-180. Three additional nonmodified peptides from synGAP were used to control for loading amounts. These peptides included VIQNLANFSK (m/z 567.3193, $z = 2$), SASGDTVFWGEHFEFNNLPAVR (m/z 827.3925, $z = 3$), and EFAEYVTNHYR (m/z 714.8308, $z = 2$). Raw data were imported into Skyline (30) for manual validation and extraction of peak areas. Statistical analysis of the variation in phosphorylation levels was carried out using MSstats (31).

Preparation of the PSD Fraction from Mouse Forebrain—The PSD fraction was prepared as described previously (32) by a modification of the method of Carlin *et al.* (33). We have been unable to extract synGAP from the PSD fraction without destroying its GAP activity.

Immunoprecipitation from Mouse Brain Membrane Fraction—Forebrains from adult male mice were homogenized with 12 up and down strokes at 900 rpm. The homogenate was cleared of membrane and nuclei by centrifuging at 1000 × g for 10 min. The supernatant was centrifuged at 100,000 × g for 1 h, and the pellet was solubilized in 1% deoxycholate. The solubilized fraction was brought to 50 mM Tris, pH 7.4, 150 mM NaCl, 1% Triton X-100, 1× Roche Applied Science protease inhibitor tablet, 0.2% deoxycholate, and the protein concentration was determined by the bicinchoninic acid method (Thermo Scientific, catalog no. 23225) with BSA as the standard. Anti-synGAP Ab (Thermo Scientific, catalog no. PA1-046, RRID, AB_2287112) or anti-rabbit IgG isotype control Ab (Upstate) (8 μg) in a final volume of 300 μl in 100 mM sodium citrate, pH 5, 0.1% Tween 20 was precoupled with 25 μl of protein G-magnetic Dynabeads (Invitrogen, catalog no. 10004D) at 4 °C overnight with end-over-end mixing. The beads were washed with 500 μl of 100 mM sodium citrate, pH 5, 0.1% Tween 20, three times for 5 min each before incubating with 1.5 mg of protein for 3 h at 4 °C. The immunoprecipitates were washed four times with 50 mM Tris, pH 7.4, 150 mM NaCl, 0.1% Triton X-100 before proteins were eluted with 1× SDS loading buffer. Samples were fractionated by SDS-PAGE on a 6% gel, and immunoblots were prepared as described above. The gel was run long enough to

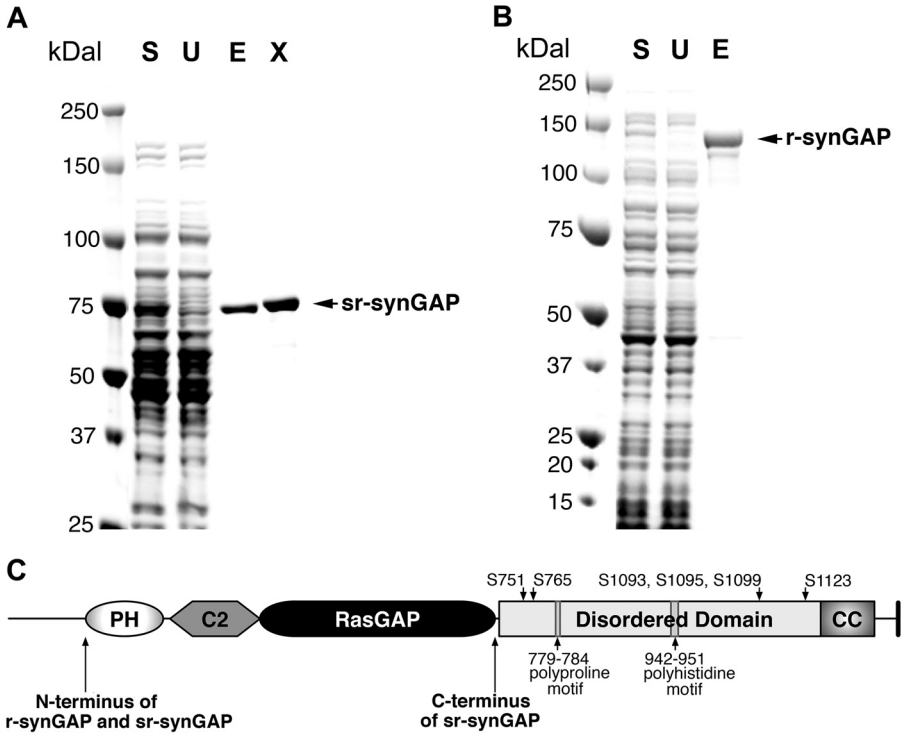

FIGURE 1. **Purification of heterologously expressed sr-synGAP and r-synGAP.** Heterologously expressed sr-synGAP and r-synGAP were purified on Talon metal affinity resin and Superdex 200 size exclusion resin as described under "Experimental Procedures." *A,* His-tagged sr-synGAP; *B,* His-tagged r-synGAP. Proteins in the indicated pools were fractionated on 4–12% gradient SDS-polyacrylamide gels and stained as described under "Experimental Procedures." *S,* soluble protein; *U,* unbound protein; *E,* eluate from Talon metal affinity columns; *X,* eluate from Superdex 200 column. *C,* domain map of synGAP; *PH*, pleckstrin homology domain (103–203); C2 domain (229–392); RasGAP, Ras GTPase-activating protein domain (393–715); disordered domain (725–1145); *CC*, coiled-coil domain (1146–1260); PDZ binding domain (1289–1293).

ensure separation of the three major splice variants of synGAP. Immunoblots were probed with α-phospho-CDK5 substrate (1:500; Cell Signaling Technology, catalog no. 2324S, RRID, AB_2244779 (discontinued, replacement catalog no. 9477)), α-total synGAP (1:2000, Thermo Scientific, catalog no. PA1-046, RRID, AB_2287112), α-PSD-95 (1:1000, Thermo Scientific Pierce Products, catalog no. MA1-046, RRID, AB_2092361), and α-GluR2 (1:1000, EMD Millipore catalog no. MAB397, RRID, AB_2113875).

Preparation and Treatment of Cortical Neuronal Cultures—Cultures of cortical neurons were prepared from fetal mice as described previously (9, 34). After 4 days *in vitro* cultures were treated with 5 μM cytosine arabinoside (Sigma, catalog no. C6645) to halt the growth of non-neuronal cells. For treatments, cultures (days *in vitro* 13–14) were washed in HEPES/control salt solution (HCSS: 20 mM HEPES, 120 mM NaCl, 5 mM KCl, 5.5 mM glucose, 0.8 mM $MgCl_2$, pH 7.4) and then exposed to 25 μM NMDA (Tocris, catalog no. 114) dissolved in HCSS (2–4 wells for each condition) for 0, 0.25, 1, 3, and 5 min. In some experiments, cultures were pretreated prior to exposure to NMDA with 30 μM roscovitine (Sigma, catalog no. R7772-5MG), 5 μM cyclosporin A (inhibits calcineurin; Sigma catalog no. 30024), 1 μM okadaic acid (inhibits PP2A strongly and PP1 weakly at this concentration; EMD, catalog no. 459620), or 500 nM tautomycin (inhibits PP1; EMD catalog no. 580551), as stated. For experiments in which CDK5 activity was inhibited with roscovitine, control wells were treated with an equal amount of vehicle (DMSO at ~0.12%). After treatment, cells were lysed, and protein concentrations were determined by the bicinchoninic acid method with BSA as the protein standard.

To measure phosphorylation of synGAP, 15–30 μg of cell lysate was fractionated by SDS-PAGE, transferred to nitrocellulose membranes, blocked, and incubated with primary antibodies as described above. Antibodies included those listed above and α-MAP-2 (1:5000, Sigma catalog no. M4403). Bound antibodies were detected with IRdye700- or IRdye800-conjugated secondary antibody (Rockland Immunochemicals catalog no. 610-130-121, RRID, AB_220121, and catalog no. 611-131-122, RRID, AB_220150) and visualized with the Odyssey infrared imaging system. Reported protein values were normalized either for staining for total synGAP or for MAP-2, as stated.

RESULTS

Purification of r-synGAP—It was previously shown that a shortened form of synGAP (sr-synGAP) comprising residues 103–725 can be expressed in soluble form in *E. coli* and that this construct displays GAP activity against Rap with a potency similar to other Rap-GAPs. In contrast, its GAP activity against Ras is considerably less potent than that of other RasGAPs (6). sr-synGAP includes the N-terminal pleckstrin homology, C2, and RasGAP domains, but it lacks residues 726–1293 that contain a predicted disordered domain containing the regulatory CaMKII phosphorylation sites (11), a short predicted coiled coil domain, and the C-terminal PDZ domain-binding motif (1, 2). To enable study of the regulatory roles of phosphorylation of purified synGAP by CaMKII and other protein kinases, we

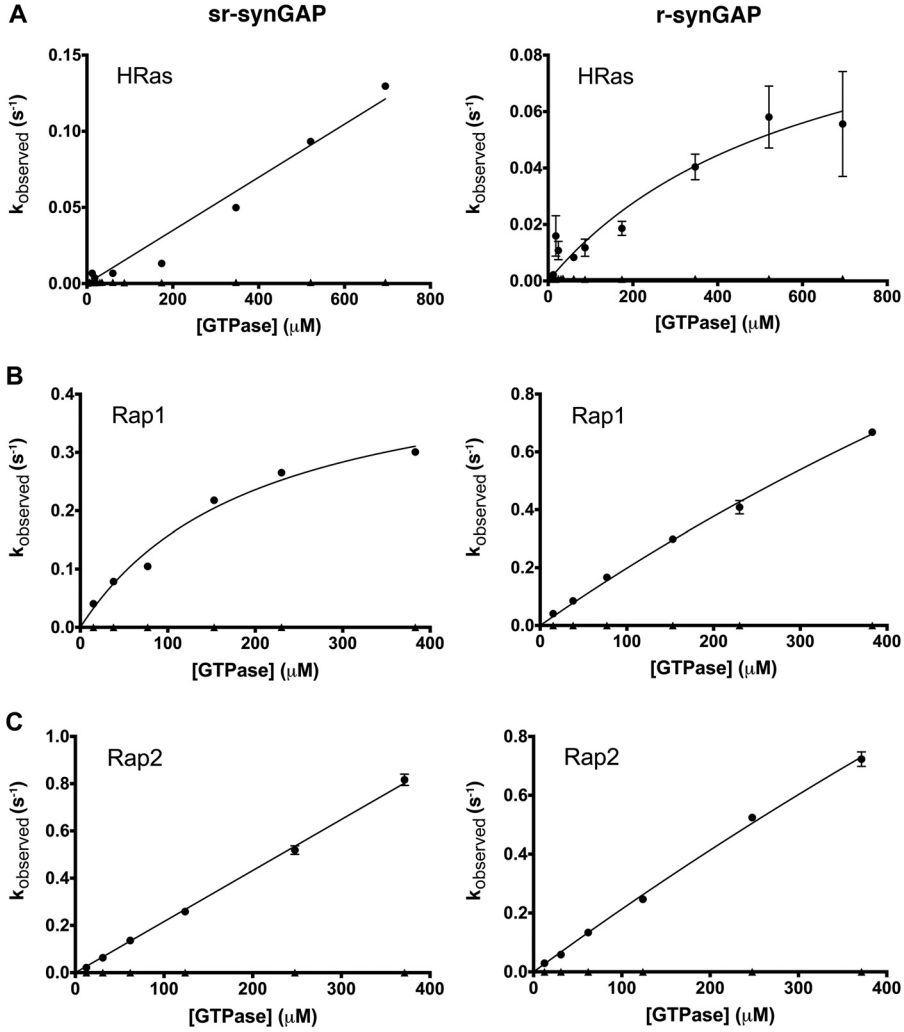

FIGURE 2. **GAP activity of sr-synGAP and r-synGAP.** GTPase activities in the presence of sr-synGAP (*left panels*) and r-synGAP (*right panels*) were measured as a function of GTPase concentration in the absence and presence of purified sr- or r-synGAP (350 nM) for 10 min at 25 °C as described under "Experimental Procedures." *A*, HRas (10–700 μM); *B*, Rap1 (15–400 μM); and *C*, Rap2 (15–400 μM). Data are mean ± S.E. ($n = 3–6$ for r-synGAP and $n = 1–2$ for sr-synGAP). The k_{obs} was calculated as moles of phosphate released per s/mol of synGAP when synGAP is present, and as moles of phosphate released per s/mol of GTPase concentration in the absence of synGAP. Note that the concentration of synGAP is much less than that of the GTPases, so the increase in k_{obs} with GTPase concentration reflects increased binding of the GTPases to limiting synGAP. See Table 1 for estimates of k_{cat} and K_m. ●, +synGAP; ▲, −synGAP.

expressed and purified a nearly full-length soluble synGAP fragment (r-synGAP; residues 103–1293) (Fig. 1*B*). We also purified sr-synGAP for comparison (Fig. 1*A*). We found that both of these shortened forms of synGAP were soluble when expressed in bacteria at low temperature (*e.g.* 18 °C), but they required addition of ATP and Mg^{2+} to release bound chaperone (GroEL) and to permit effective binding of the recombinant protein to Talon metal affinity columns during purification (data not shown). A combination of immobilized metal affinity chromatography and SEC was used to purify the synGAP constructs as described under "Experimental Procedures." sr-synGAP was purified to >95% purity, with typical yields in excess of 75%. r-synGAP was purified by immobilized metal affinity chromatography alone to ~70% purity, with yields in excess of 85%. r-synGAP eluted in the void volume of SEC columns with no improvement in purity, suggesting that the presence of the disordered domain and/or the coiled-coil domain may predispose r-synGAP to multimerization. Fig. 1*C* is a domain map of synGAP showing the boundaries of the two recombinant forms and the positions of previously identified phosphorylation sites.

Intrinsic GAP Activity of r-synGAP—synGAP has been shown to stimulate the GTPase activity of Rap much more potently than that of Ras (5, 6). sr-synGAP, containing the pleckstrin homology, C2, and Ras GAP domains, was found to stimulate the intrinsic GAP activity of Rap1 by 4 orders of magnitude, to a k_{cat} of 0.8 s^{-1}, and that of HRas by 2 orders of magnitude (6).

We attempted to measure the enzymatic constants for the acceleration of GAP activity of HRas, Rap1, and Rap2 by limiting amounts of r-synGAP or sr-synGAP (Fig. 2 and Table 1). In our assay, both synGAP constructs stimulated the rate of GTP hydrolysis by HRas by 2 orders of magnitude (Fig. 2*A*), consistent with previous findings (6). Stimulation of GTPase activity by sr-synGAP varied approximately linearly with HRas concentration in the range that we were able to test (10–700 μM). Therefore, we were not able to estimate k_{cat} or K_m values. At 700 μM HRas, k_{obs} in the presence of sr-synGAP was 0.13 s^{-1}. In

TABLE 1

Intrinsic GAP activities of r-synGAP

K_m and k_{cat} values of HRas, Rap1, and Rap2, in the absence and presence of sr-synGAP and r-synGAP, are estimated from data in Fig. 2 fitted by nonlinear regression in Prism as described under "Experimental Procedures." Error is S.E. NF, could not be determined from fit.

GTPase	Enzyme	K_m	k_{cat}	-Fold stimulation
		μM	s^{-1}	
HRas	GTPase alone		$7.7 \times 10^{-4} \pm 3 \times 10^{-5}$	
	+ sr-synGAP	NF	0.13[a]	170[a]
	+ r-synGAP	640 ± 400	0.12 ± 0.05	150
Rap1	GTPase alone		$1.1 \times 10^{-4} \pm 1 \times 10^{-5}$	
	+ sr-synGAP	200 ± 55	0.47 ± 0.06	4300
	+ r-synGAP	1800 ± 600	3.8 ± 1.1	35,000
Rap2	GTPase alone		$7.9 \times 10^{-5} \pm 9 \times 10^{-6}$	
	+ sr-synGAP	NF	0.82[b]	10,400[b]
	+ r-synGAP	3100 ± 1500	6.8 ± 3.0	87,000

[a] k_{obs}, data observed at 700 μM HRas.
[b] k_{obs}, data observed at 400 μM Rap.

contrast, stimulation of HRas GTPase by r-synGAP varied nonlinearly with HRas concentration and could be fit by a hyperbolic curve, permitting estimation of $k_{cat} = 0.12 \pm 0.05\ s^{-1}$ and $K_m = 640 \pm 400\ \mu M$. The error of these calculations is high; thus, they can only be considered estimates.

Stimulation of GTPase activity of Rap1 by both sr-synGAP and r-synGAP followed a hyperbolic curve with increasing Rap1 concentrations (Fig. 2*B*). For sr-synGAP, we calculated $k_{cat} = 0.47 \pm 0.06\ s^{-1}$, which is in reasonable agreement with the value of $0.8\ s^{-1}$ reported by Pena *et al.* (6), and $K_m = 200 \pm 55\ \mu M$. r-synGAP stimulated the GTPase activity of Rap1 to a k_{cat} of $3.8 \pm 1.1\ s^{-1}$, which is greater than the stimulation by sr-syn-GAP. However, the affinity of r-synGAP for Rap1 appeared considerably lower ($K_m = 1800 \pm 600\ \mu M$) than that of sr-synGAP. The fold stimulations of Rap1 GTPase activity by sr-synGAP and r-synGAP were 4300 and 35,000, respectively. These results suggest that the carboxyl portion of r-synGAP (residues 726–1293) alters the interaction of synGAP with Rap1, producing a lower affinity, but a greater maximum stimulation of its GTPase activity.

Stimulation of GTPase activity of Rap2 by sr-synGAP was linear over the range of Rap2 concentrations we were able to test (15–400 μM), again precluding estimation of k_{cat} and K_m values (Fig. 2*C*). r-synGAP stimulated Rap2 GTPase to approximately the same rate as did sr-synGAP. However, for r-synGAP, the plot of k_{obs} against the Rap2 concentration was slightly hyperbolic, permitting rough estimates of $k_{cat} = 6.8 \pm 3\ s^{-1}$ and $K_m = 3100 \pm 1500\ \mu M$. This represents a stimulation of GTP hydrolysis in the presence of r-synGAP of ~87,000-fold over the rate of hydrolysis by Rap2 alone (Table 1). Because we could not calculate a k_{cat} for sr-synGAP, it is not clear whether the carboxyl-half of r-synGAP alters its interaction with Rap2 as it appears to with Rap1.

Our measured K_m values are relatively high compared with many other enzymes, indicating a relatively low affinity of synGAP for the GTPases. However, other dual specificity GAPs and Rap GAPs have K_m values in the range of tens to a few hundred micromolars (15, 22). A high K_m value can be advantageous because it permits a linear response of catalytic rate over a wide range of substrate concentrations (35). The importance of this property in spine synapses is not clear because the effective concentrations of activated Ras or Rap in the confined space of the postsynaptic density after different *in vivo* stimuli are not known.

Stoichiometry and Rate of r-synGAP Phosphorylation by CDK5—Preliminary mass spectrometric analysis of synGAP in the PSD fraction had revealed phosphorylation at Ser-773 within a motif recognized by CDK5 (data not shown). Therefore, we tested whether purified CDK5 could phosphorylate purified r-synGAP *in vitro*. Under the conditions of our assay (Fig. 3*A*), phosphorylation of r-synGAP by CDK5 was approximately linear with time for 10 min, after which r-synGAP contained ~0.3 to 0.4 mol of phosphate/mol. By 60 min, the stoichiometry approached an asymptote of 1 mol of phosphate/mol of r-synGAP.

Phosphorylation of 0.3 μM r-synGAP by CDK5/p35 occurred at a similar rate (0.03 mol of phosphate/mol of substrate/min) as phosphorylation of the CDK5 substrate histone H1 at a concentration of 4.3 μM (data not shown). These results indicate that r-synGAP is at least as good a substrate for CDK5 as histone H1.

Identification of Sites in r-synGAP Phosphorylated by CDK5—We used sensitive proteomic mass spectrometric methods to identify all sites on r-synGAP phosphorylated by CDK5. r-synGAP was incubated with CDK5/p35 for 2 or 10 min and quenched with LDS stop buffer as described under "Experimental Procedures." Following separation by SDS-PAGE, phosphorylated r-synGAP was reduced, alkylated, and digested in the gel with trypsin as described under "Experimental Procedures." Tryptic peptides were fractionated by nano-LC and analyzed on a hybrid mass spectrometer equipped with a linear ion trap in combination with Fourier transform ion cyclotron resonance. Ions collected in the linear ion trap were fragmented by collision-induced dissociation (MS2) as described under "Experimental Procedures." If a neutral loss of 32.67, 49.00, or 97.97 Da was observed in MS2, an MS3 neutral loss scan was acquired to detect the presence of dehydroalanine at phosphorylation sites, resulting from the β-elimination of H_3PO_4 from phosphoserine. Following completion of data collection and analysis via Mascot, as described under "Experimental Procedures," results were stringently filtered to a protein probability of 99%, a two peptide minimum, and a peptide probability of 95% in Scaffold as described under "Experimental Procedures." The predicted false localization rate of phosphorylation site

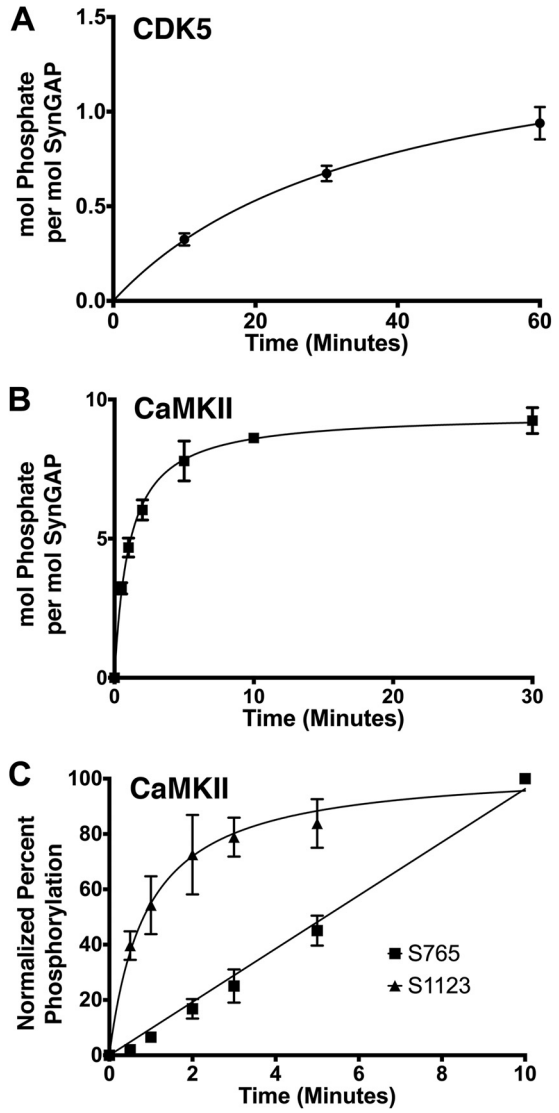

FIGURE 3. **Stoichiometry of phosphorylation of r-synGAP by CDK5 and CaMKII.** *A,* stoichiometry of phosphorylation by CDK5/p35. r-synGAP (286 nM) was incubated in the presence of CDK5/p35 (110 nM) and 500 μM [γ-^{32}P]ATP (375 cpm/pmol), as described under "Experimental Procedures." At the indicated times, reactions were quenched by addition of 4× LDS sample buffer. Radiolabeled r-synGAP was isolated by SDS-PAGE on 4–12% gels and visualized with a PhosphorImager as described under "Experimental Procedures." The content of labeled phosphate in the r-synGAP protein band was quantified with the use of ImageQuant TL software. *B,* stoichiometry of r-synGAP phosphorylation by CaMKII. r-synGAP (286 nM) was phosphorylated in the presence of CaMKII (3.1 nM), 500 μM [γ-^{32}P]ATP (100 cpm/pmol), 0.7 mM $CaCl_2$, and 3.4 μM calmodulin (*CaM*) as described under "Experimental Procedures." Labeled synGAP was quantified as described for *A*. *C,* phosphorylation by CaMKII of individual sites on r-synGAP. r-synGAP (286 nM) was phosphorylated as described in *B*, with cold ATP in place of [γ-^{32}P]ATP. Following fractionation by SDS-PAGE, r-synGAP was transferred to PVDF membranes and probed with anti-phospho-synGAP-Ser-764/5 and anti-phospho-synGAP-Ser-1123, as described under "Experimental Procedures." Staining was quantified on a Li-Cor imager as described under "Experimental Procedures." Intensity of staining for phosphorylated Ser-765 and Ser-1123 was normalized for each to the value at 10 min. All data are mean ± S.E. (n = 4).

identifications was then assessed for each phosphopeptide using the Mascot Delta score as described previously (27). Peptide sequence coverage of r-synGAP was in excess of 84%, with 90% coverage of the disordered domain (91.9% theoretical maximum coverage of r-synGAP calculated by ExPASy Peptide Mass Program). We found no phosphorylated sites on r-synGAP before it was incubated with CaMKII or CDK5.

TABLE 2
Identification of CDK5 phosphorylation sites in r-synGAP

Residues marked with an *X* are CDK5 phosphorylation sites in r-synGAP identified as described under "Experimental Procedures." Phosphorylated residues are categorized according to the length of the phosphorylation reaction (2 and 10 min) and their detection in MS2 or MS3 spectra. The sites highlighted with an asterisk have phosphorylation false localization rates less than 1% (predicted as described under "Experimental Procedures").

Residue phosphorylated	2 min		10 min	
	MS2	MS3	MS2	MS3
Ser-728	*X**	*X**	*X**	*X**
Ser-773	*X**	*X**	*X**	*X**
Thr-775	*X*	*X*	*X*	*X*
Ser-802	*X*	*X*	*X*	*X*
Ser-842	*X**		*X*	*X*

We confirmed that Ser-773 and Ser-802 are phosphorylated by CDK5, and we detected three additional sites (Ser-728, Thr-775, and Ser-842) (Table 2 and supplemental data). Of the identified CDK5 phosphorylation sites, only Ser-773 and Ser-802 are located in a consensus motif for phosphorylation by CDK5 ((S/T)P). Ser-773 is contained in a favored CDK5 consensus sequence with a Lys at the +3 position (SP*X*(R/K)). Although Ser-773 had a predicted phosphorylation false localization rate of less than 1%, Ser-802 had a predicted rate greater than 5% because it has a neighboring serine. However, close inspection of mass spectra from peptides that are predicted to be phosphorylated at Ser-802, and high mascot scores (~65–85) for their MS2 and MS3 spectra, confirmed the presence of phosphorylation at Ser-802. Because of its close proximity to Ser-773, phosphorylation at Thr-775 may serve the same regulatory function as Ser-773, and/or its phosphorylation may result from promiscuity of the enzymatic phosphorylation. We chose to focus our efforts on Ser-773 and Ser-802 because of their localization within CDK5 consensus sequences and their phosphorylation in synGAP within the PSD (see below). However, we note that Ser-728 and Ser-842 may also be legitimate CDK5 phosphorylation sites.

Stoichiometry and Rate of r-synGAP Phosphorylation by CaMKII—In preparation for comparison of the effects of phosphorylation of r-synGAP by CDK5 and CaMKII, we examined the time course of phosphorylation of r-synGAP by CaMKII. As we found previously for full-length synGAP (11), r-synGAP is phosphorylated rapidly and to a high stoichiometry by CaMKII (Fig. 3*B*). The most rapid phosphorylation occurs within 2 min, after which r-synGAP contains ~6 mol of phosphate/mol, indicating that there are many phosphorylation sites recognized by CaMKII. After 10 min, the rate reaches an asymptote at a stoichiometry of ~9 mol of phosphate/mol. Because our GAP assays are inhibited by concentrations of ATP in excess of 30 μM, we compared the stoichiometry of r-synGAP phosphorylation by CaMKII at 30 and 500 μM ATP. Reaction mixtures containing 30 μM ATP followed the same reaction profile as reactions with 500 μM ATP; however, the overall stoichiometry plateaued at ~6.5 mol of phosphate incorporated per pmol of r-synGAP (data not shown). The stoichiometry and time course of phosphorylation of r-synGAP by CaMKII in 30 μM ATP were nearly identical to those of phosphorylation

TABLE 3

Identification of CaMKII phosphorylation sites in r-synGAP

Residues marked with an *X* are CaMKII phosphorylation sites in r-synGAP identified as described under "Experimental Procedures." Phosphorylated residues are categorized according to the length of the phosphorylation reaction (2 and 10 min) and detection in MS2 or MS3 spectra. The sites highlighted with an asterisk have phosphorylation false localization rates less than 1% (predicted as described under "Experimental Procedures").

Residue modified	2 min		10 min	
	MS2	MS3	MS2	MS3
Ser-728			*X*	*X*
Ser-737	*X**	*X**	*X**	*X**
Ser-750			*X*	
Ser-751	*X**		*X**	
Ser-756			*X*	
Ser-764	*X*			
Ser-765	*X**	*X**	*X**	*X**
Ser-808	*X*		*X*	
Ser-809	*X*		*X*	
Ser-810	*X*		*X*	
Ser-821	*X**		*X**	
Ser-825	*X**	*X**	*X**	*X**
Ser-827	*X**	*X**	*X**	*X**
Ser-842	*X*			
Ser-843	*X*			
Ser-882	*X**	*X**	*X**	*X**
Ser-883	*X**	*X**	*X**	
Thr-885			*X**	
Ser-892			*X**	
Thr-897	*X**	*X**	*X**	*X**
Thr-898	*X*	*X*		*X*
Ser-990	*X*	*X*	*X*	
Ser-1093	*X**		*X**	
Ser-1095	*X**		*X**	
Ser-1099	*X**	*X**	*X**	*X**
Ser-1123	*X**		*X**	
Ser-1150	*X**	*X**	*X**	
Ser-1171		*X*	*X*	*X*
Ser-1210	*X**	*X**	*X**	*X**
Ser-1283	*X**	*X**	*X**	*X**
Thr-1291			*X**	

reactions carried out with endogenous synGAP and CaMKII in the PSD fraction (11).

Phosphorylation of r-synGAP by CaMKII (Fig. 3*B*) proceeded more rapidly and to a higher stoichiometry than phosphorylation by CDK5 (Fig. 3*A*), despite the fact that reaction mixtures for CaMKII contained a 100:1 molar ratio of r-synGAP (substrate) to kinase, whereas those for CDK5 contained a 2:1 molar ratio of r-synGAP to kinase.

To compare the rate of phosphorylation of two previously identified sites on r-synGAP by CaMKII, we used phosphosite-specific antibodies developed against phosphorylated peptides containing Ser-765 and Ser-1123 (11). We measured phosphorylation of the two sites by Western blotting as described under "Experimental Procedures" (Fig. 3*C*). Ser-1123 was phosphorylated very rapidly, to ~70% of maximum in the first 2 min and reaching a plateau by 10 min. Ser-765 was phosphorylated more slowly at a linear rate reaching a maximum at 10 min.

Identification of Sites in r-synGAP Phosphorylated by CaMKII—We identified all sites of phosphorylation of r-synGAP by CaMKII using the same sensitive proteomic mass spectrometric methods described above. We confirmed the presence of six CaMKII phosphorylation sites previously identified by our laboratory (Ser-751, Ser-765, Ser-1093, Ser-1095, Ser-1099, and Ser-1123) (Table 3 and supplemental data). We also identified 10 additional phosphorylation sites in r-synGAP (Ser-737, Ser-821, Ser-825, Ser-827, Ser-882, Ser-883, Thr-897, Ser-1150, Ser-1210, and Ser-1283) (Table 3 and supplemental data). All of these sites were detected at both the 2- and 10-min time points and had false localization rates of less than 1%. Phosphorylation was detected at sites Ser-750, Ser-756, and Ser-764, primarily at 10 min; however, the phosphorylation false localization rates at these sites were >5%. Because sites Ser-737, Ser-751, Ser-765, Ser-1093, Ser-1095, Ser-1099, Ser-1123, Ser-1150, Ser-1210, and Ser-1283 had false localization rates under 1%, we believe that these 10 serines are all candidates for sites of phosphorylation of r-synGAP by CaMKII. We detected a large number of phosphorylation sites between residues 800 and 900 suggesting that this region may be exposed to the protein surface and/or particularly disordered. Either circumstance could lead to promiscuous phosphorylation of serine and threonine residues in this region.

Effect of CDK5 Phosphorylation on GAP Activity of r-synGAP—We measured GAP activity of r-synGAP before and after phosphorylation by CDK5 for 1, 2, 5, and 10 min as described under "Experimental Procedures" (Fig. 4, *A–C*). Phosphorylation by CDK5 increased the HRas (Fig. 4*A*) GAP activity of r-synGAP substantially (98%) and the Rap1 (Fig. 4*B*) GAP activity slightly (20%), but it did not increase Rap2 GAP activity (Fig. 4*C*). The effect of CDK5 on HRas reached significance after 2 min and plateaued at 5 min. The effect on Rap1 was nearly maximal (15%) after 1 min. These data show that phosphorylation of r-synGAP by CDK5 accelerates its rate of inactivation of HRas considerably more potently than its inactivation of Rap1.

Effect of CaMKII Phosphorylation on GAP Activity of r-synGAP—We measured GAP activity of r-synGAP before and after phosphorylation by CaMKII as described under "Experimental Procedures" (Fig. 4, *D–F*). In contrast to CDK5, phosphorylation by CaMKII increased the HRas (Fig. 4*D*) GAP activity of r-synGAP slightly (25%) and the Rap1 (Fig. 4*E*) GAP activity of r-synGAP substantially (76%). Like CDK5, it did not increase its Rap2 GAP activity (Fig. 4*F*). CaMKII phosphorylation of r-synGAP produced a gradual increase in Ras GAP activity, plateauing at 10 min. In contrast, Rap1 GAP activity increased to near its maximum level after 1 min (61%) of phosphorylation by CaMKII. Thus, phosphorylation of r-synGAP by CaMKII accelerates its rate of inactivation of Rap1 more potently than its rate of inactivation of HRas.

Phosphorylation by CDK5 or CaMKII Alters the Ratio of HRas GAP and Rap1 GAP Activities of r-synGAP—The intrinsic rate of hydrolysis of GTP by HRas (~0.0004–0.0008 s^{-1}) (36) is ~7–10 times faster than that of Rap1 (~0.00005–0.0001 s^{-1}) (37). However, unphosphorylated r-synGAP and endogenous synGAP (5) stimulate Rap's GTP hydrolysis much more potently than that of Ras (5, 6). In our experiments, unphosphorylated r-synGAP caused Rap1 to be inactivated at a rate ~3.9 times faster than HRas (Fig. 5). Phosphorylation by CDK5 or CaMKII shifts this ratio significantly. Phosphorylation by CDK5 for 10 min decreases it to ~2.2 by preferentially increasing stimulation of HRas GAP activity. Conversely, phosphorylation by CaMKII increases the ratio to ~5.5 by preferentially increasing stimulation of Rap1 GAP activity.

Regulation of GAP Activity of r-synGAP Mutants—To determine which CDK5 phosphorylation sites are responsible for the effects of phosphorylation on GAP activity, we created mutations in r-synGAP at sites Ser-773 and Ser-802, as well as at

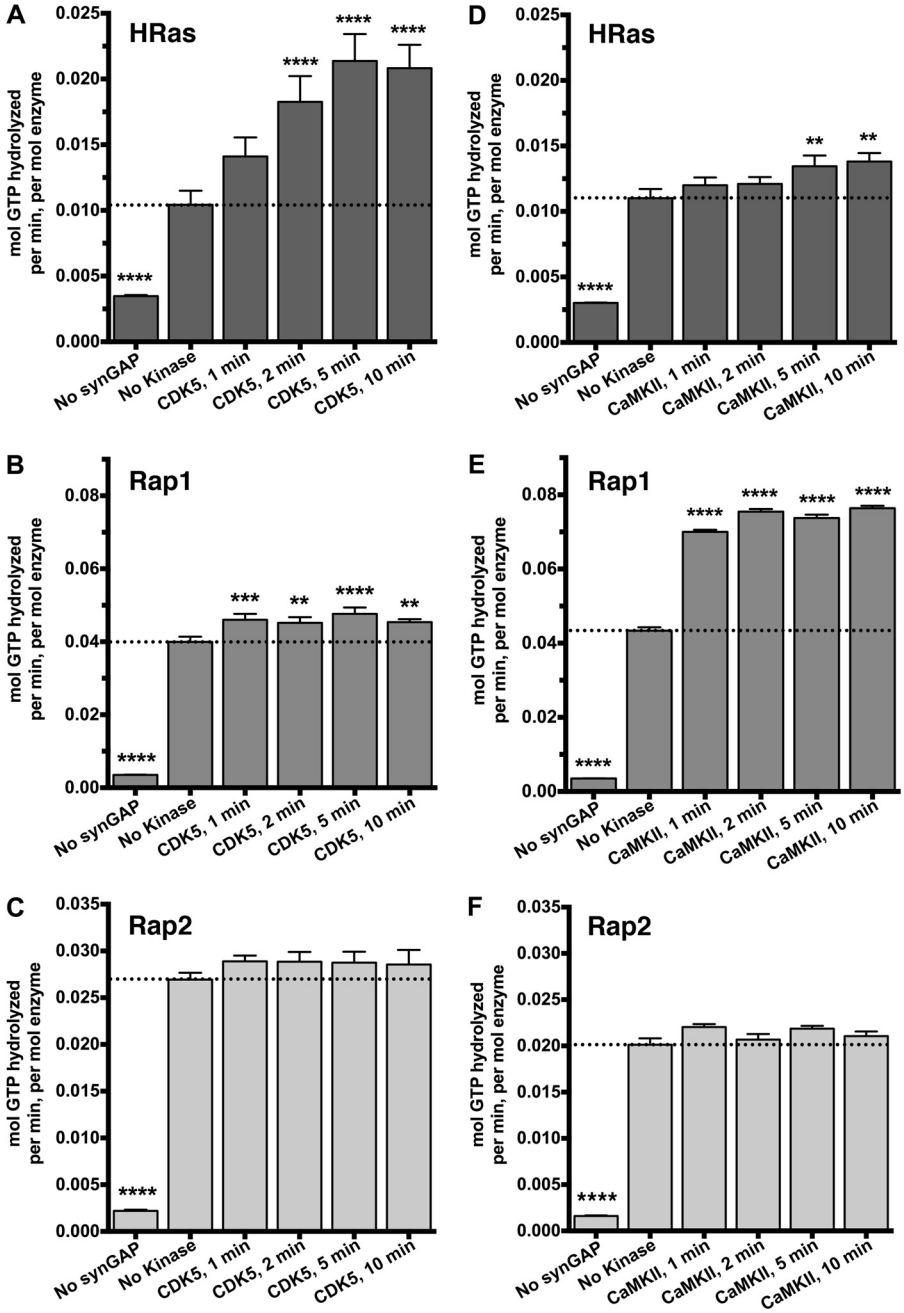

FIGURE 4. **Effect of CDK5 or CaMKII phosphorylation on GAP activity of r-synGAP.** r-synGAP was phosphorylated for 1–10 min in the presence of CDK5/p35 or CaMKII as described under "Experimental Procedures." In the phosphorylation reactions, the synGAP, CDK5, and CaMKII concentrations were 2.5, 2.1, and 3.2 times higher, respectively, than in the reactions shown in Fig. 3. GAP activities of control and phosphorylated r-synGAP (250 nM) were then measured by incubation with [γ-^{32}P]GTP-loaded GTPases for 10 min at 25 °C as described under "Experimental Procedures." *A,* HRas GAP activity; *B,* Rap1 GAP activity; and *C,* Rap2 GAP activity following phosphorylation by CDK5. *D,* HRas GAP activity; *E,* Rap1 GAP activity; and *F,* Rap2 GAP activity following phosphorylation by CaMKII. Initial rates were measured at 10 min; GTPase activity was linear for 25 min (data not shown). Data are mean ± S.E. (*A–C,* $n = 10$; *D–F*, $n = 9$). The statistical significance of differences from the GTPase activity of unphosphorylated r-synGAP (*No Kinase*) was determined by ordinary one-way ANOVA (uncorrected Fisher's LSD). **, $p < 0.01$; ***, $p < 0.001$; ****, $p < 0.0001$. *Dotted lines* indicate the levels of GTPase activity in the presence of unphosphorylated synGAP.

combinations of other phosphorylation sites. The sites were mutated to alanine to prevent their phosphorylation (phosphodeficient) or to aspartic acid to mimic the effect of phosphorylation by adding a negative charge (phosphomimetic). Mutants were purified by the same procedure as wild type r-synGAP as described under "Experimental Procedures."

We first measured the HRas and Rap1 GAP activities of the mutants (Fig. 6). As expected, mutations T775A and S802A did not affect the GAP activity of r-synGAP. Unexpectedly, mutation S773A and the double mutation S773A/T775A resulted in significantly reduced stimulation of GAP activity compared with the wild type construct. This effect was most pronounced for Rap2 GAP activity (Fig. 6*C*), least pronounced for Rap1 GAP activity (Fig. 6*B*), and intermediate for HRas GAP activity (Fig. 6*A*). In contrast, the triple mutation S773A/T775A/S802A produced an increase in HRas and Rap2 GAP activities (Fig. 6, *A*

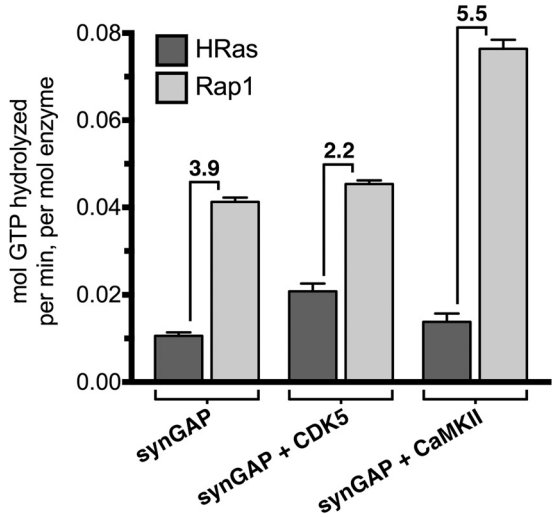

FIGURE 5. **Alteration of the ratio of HRas GAP and Rap1 GAP activities of r-synGAP after phosphorylation by CDK5 or CaMKII.** Data from Fig. 4 are re-plotted to emphasize the change in ratio of HRas GAP and Rap1 GAP activities after phosphorylation of r-synGAP for 10 min by CDK5 or CaMKII. The data for unphosphorylated r-synGAP from Fig. 4 were combined. The *numbers* above each bracket are the ratios of the means of Rap1 GAP activity to HRas GAP activity for each pair of conditions. Plotting the data for HRas and Rap1 on the same axis emphasizes r-synGAP's greater stimulation of GTP hydrolysis by Rap1 compared with HRas. Note that, in the absence of synGAP, Rap1 has a lower rate of GTP hydrolysis than HRas (Table 1).

and *C*) and did not affect Rap1 GAP activity (Fig. 6*B*). These data suggest that mutation of Ser-773 to alanine disrupts folding of synGAP in a way that reduces catalysis; however, mutation of Ser-802 to alanine abrogates this effect and even stimulates catalysis. These two phosphorylation sites flank a 6-residue polyproline motif (Fig. 1*C*), which can form a relatively rigid rod-like structure. It is possible that mutation of serines, or their phosphorylation, on either side of this motif have a particularly powerful effect on the position of the disordered domain in relation to the GAP catalytic domain and thus alter GAP activity.

The CTM-Plus mutant of r-synGAP, described under "Experimental Procedures," in which serines and threonines at positions 750, 751, 756, 764, 765, 1058, 1062, 1064, 1093, 1095, 1099, 1123, and 1125 are all mutated to alanine, closely resembles mutant S773A in its enzymatic behavior. This suggests that bulk mutagenesis of serines and threonines to alanine in the disordered domain alters protein folding in a way similar to the mutation S773A.

Single and double phosphomimetic mutations S773D, T775D, and S773D/T775D completely inhibited HRas and Rap2 GAP activities, suggesting that phosphorylation of Ser-773 or Thr-775 may be inhibitory. However, the inhibition of Rap1 GAP activity by these mutations was small. In contrast, the S802D mutant and the double mutant S773D/S802D increased all three GAP activities above that of wild type, HRas (~25%),

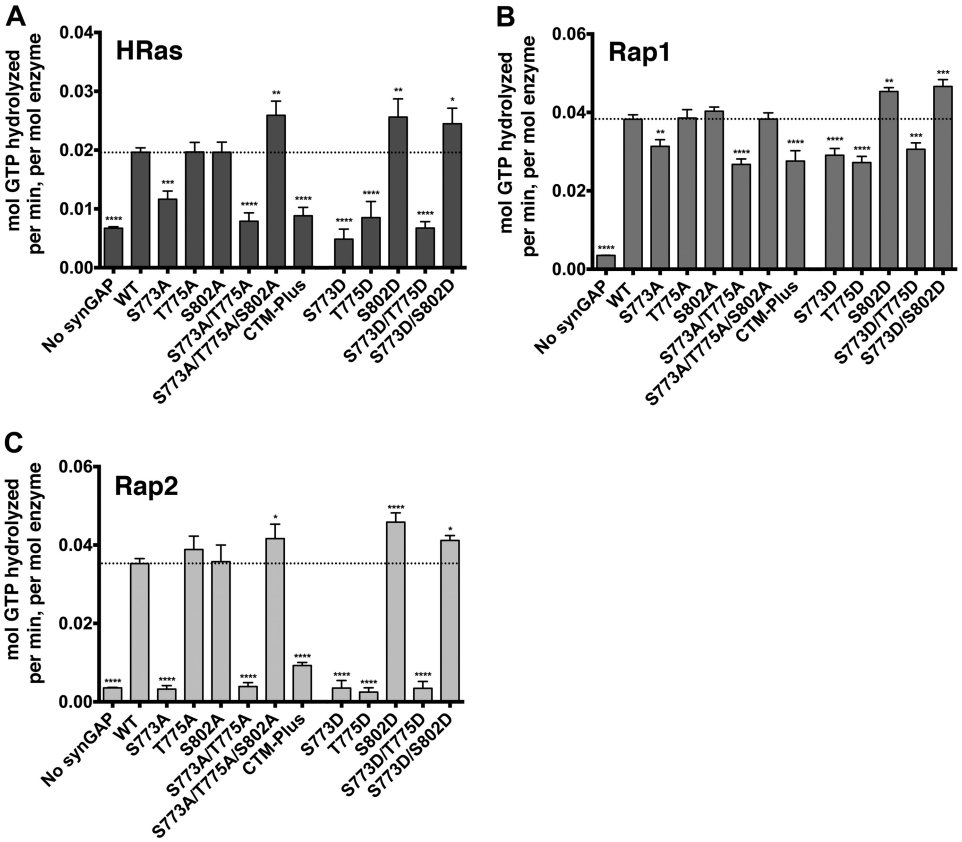

FIGURE 6. **Intrinsic GAP activities of alanine and aspartic acid mutants of r-synGAP.** GAP activities of wild type and mutant r-synGAP (250 nM) were measured by incubation with [γ-^{32}P]GTP-loaded GTPases for 10 min at 25 °C as described under "Experimental Procedures." *A,* HRas GAP activity; *B,* Rap1 GAP activity; and *C,* Rap2 GAP activity. Proteins are named according to their specific point mutations (as described under "Experimental Procedures"). Initial rates were measured at 10 min; GTPase activity was linear for 25 min (data not shown). Data are mean ± S.E. ($n = 5$). The statistical significance of differences from the GTPase activity of wild type r-synGAP (*WT*) was determined by ordinary one-way ANOVA (uncorrected Fisher's LSD). *, $p < 0.05$; **, $p < 0.01$; ***, $p < 0.001$; ****, $p < 0.0001$. *Dotted lines* indicate the levels of GTPase activity in the presence of wild type synGAP.

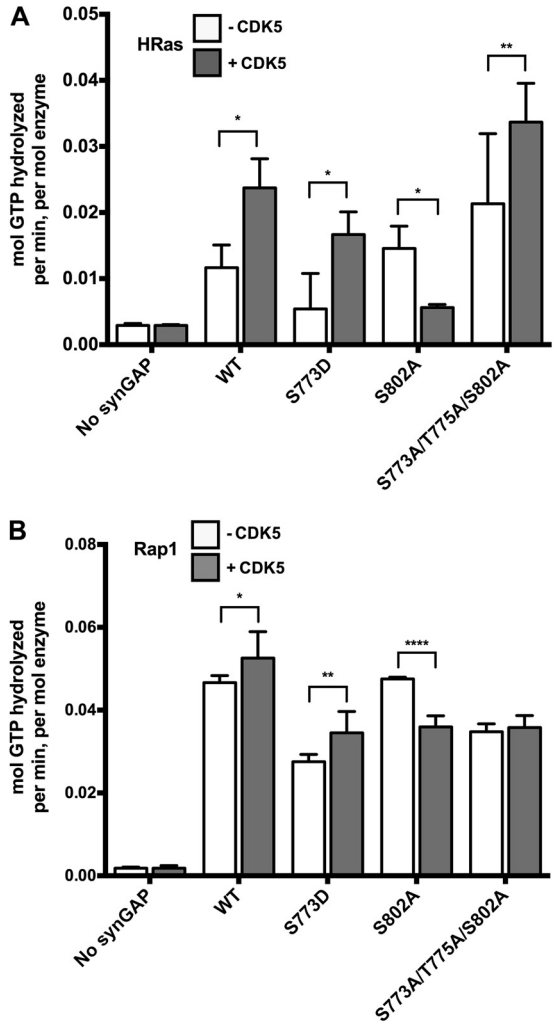

FIGURE 7. **Effect of CDK5 phosphorylation on the GAP activities of selected alanine and aspartic acid mutants of r-synGAP.** Wild type and mutant r-synGAP were phosphorylated for 10 min in the presence of CDK5/p35 as described in Fig. 4, *A* and *B*. Initial rates of GAP activities for control and phosphorylated r-synGAP (250 nM) were then measured by incubation with [γ-^{32}P]GTP-loaded GTPases for 10 min at 25 °C. GTPase activity was linear for 25 min (data not shown). *A,* HRas GAP activity; and *B,* Rap1 GAP activity. Proteins are named according to their specific point mutations as in Fig. 7. Data are mean ± S.E. ($n = 6–7$). The statistical significance of differences between GTPase activity of unphosphorylated and phosphorylated r-synGAP was determined by ordinary one-way ANOVA (uncorrected Fisher's LSD). *, $p < 0.05$; **, $p < 0.01$; ****, $p < 0.0001$.

Rap1 (~20%), and Rap2 (30 and 17%, respectively). This result suggests that phosphorylation of Ser-802 may enhance GAP activity.

When compared with Fig. 4, the data indicate that phosphomimetic mutants of r-synGAP at these three sites do not accurately reproduce the effects of phosphorylation by CDK5. However, they do suggest that phosphorylation at Ser-773/Thr-775 might inhibit GAP activity of r-synGAP, whereas phosphorylation at Ser-802 might increase it. They also suggest that phosphorylation of both sites at the same time would produce a net increase in GAP activity.

We further tested this hypothesis by phosphorylating the S773D r-synGAP mutant with CDK5. Before phosphorylation, this mutant has no HRas GAP activity and reduced Rap1 GAP activity. We predicted that CDK5 would phosphorylate Ser-802 in the mutant and that this would increase HRas and Rap1 GAP activities. As predicted, HRas GAP activity was increased by 220% and Rap1 GAP activity by 9% after phosphorylation (Fig. 7). In comparison, phosphorylation of WT synGAP with CDK5 increased HRas GAP activity 98% and Rap1 GAP activity 20%, supporting the conclusion that phosphorylation of Ser-802 may account for a major portion of the differential regulation of HRas and Rap GAP activities by CDK5.

We also predicted that phosphorylation of the S802A mutant by CDK5 would result primarily in phosphorylation at Ser-773, causing a decrease in HRas and Rap1 GAP activities, as we had observed for the S773D mutant. Again, as predicted, phosphorylation of the S802A mutant with CDK5 caused a 61% decrease in HRas GAP activity and a 9% decrease in Rap1 GAP activity, supporting the inhibitory role of phosphorylation at Ser-773.

To determine whether additional, noncanonical CDK5 phosphorylation sites play a role in regulating GAP activity, we phosphorylated the S773A/T775A/S802A triple mutant in the presence of CDK5, which should cause phosphorylation at one or both of the noncanonical sites, Ser-728 and Ser-842, which had been detected by mass spectrometry (Table 2). The phosphorylation produced a 57% increase in HRas GAP activity and no significant change in Rap1 GAP activity. These results suggest that noncanonical phosphorylation sites do indeed play a role in regulation of HRas GAP activity by CDK5. They may act together with Ser-802 to regulate HRas and Rap1 GAP activities by a combinatorial mechanism. An understanding of the structural basis of this complex regulation of GAP activity by phosphorylation of the disordered domain will require additional structural studies.

Phosphorylation of Ser-773 and Ser-802 in the PSD Fraction from Mouse Brain—To test whether CDK5 phosphorylates synGAP *in vivo* in the PSD, we looked for phosphorylation of Ser-773 and Ser-802 on endogenous synGAP in the PSD fraction from mouse brain. We incubated mouse PSD fractions in the absence and presence of Mg^{2+}/ATP, exogenous CDK5/p35, and roscovitine, as described under "Experimental Procedures". Proteins were fractionated by SDS-PAGE, and the 140–160-kDa bands containing synGAP were excised for tryptic digestion. Coupled liquid chromatography and hybrid quadrupole-Orbitrap mass spectrometric analysis of the digests confirmed that Ser-773 and Ser-802 are phosphorylated in isolated PSDs without addition of exogenous kinase (Fig. 8, *A* and *B*) and are phosphorylated concurrently when exogenous CDK5/p35 is added to the PSD (Fig. 8, *C* and *D*). Addition of Mg^{2+}/ATP to the PSD did not significantly change the amount of phosphorylation at either site; however, simultaneous addition of purified CDK5/p35 and Mg^{2+}/ATP increased the phosphorylation of both sites substantially, indicating that both sites are accessible to phosphorylation by CDK5 in the PSD. Addition of the CDK5 inhibitor roscovitine with exogenous CDK5/p35 prevented additional phosphorylation at both sites, indicating that CDK5 is the primary kinase responsible for phosphorylation of Ser-773 and Ser-802 in these experiments.

NMDA Receptor-dependent Activity Differentially Regulates Phosphorylation of synGAP at Ser-773 (CDK5) and at Ser-765 and Ser-1123 (CaMKII)—We used a commercially available antibody that recognizes CDK5 substrates phosphorylated on

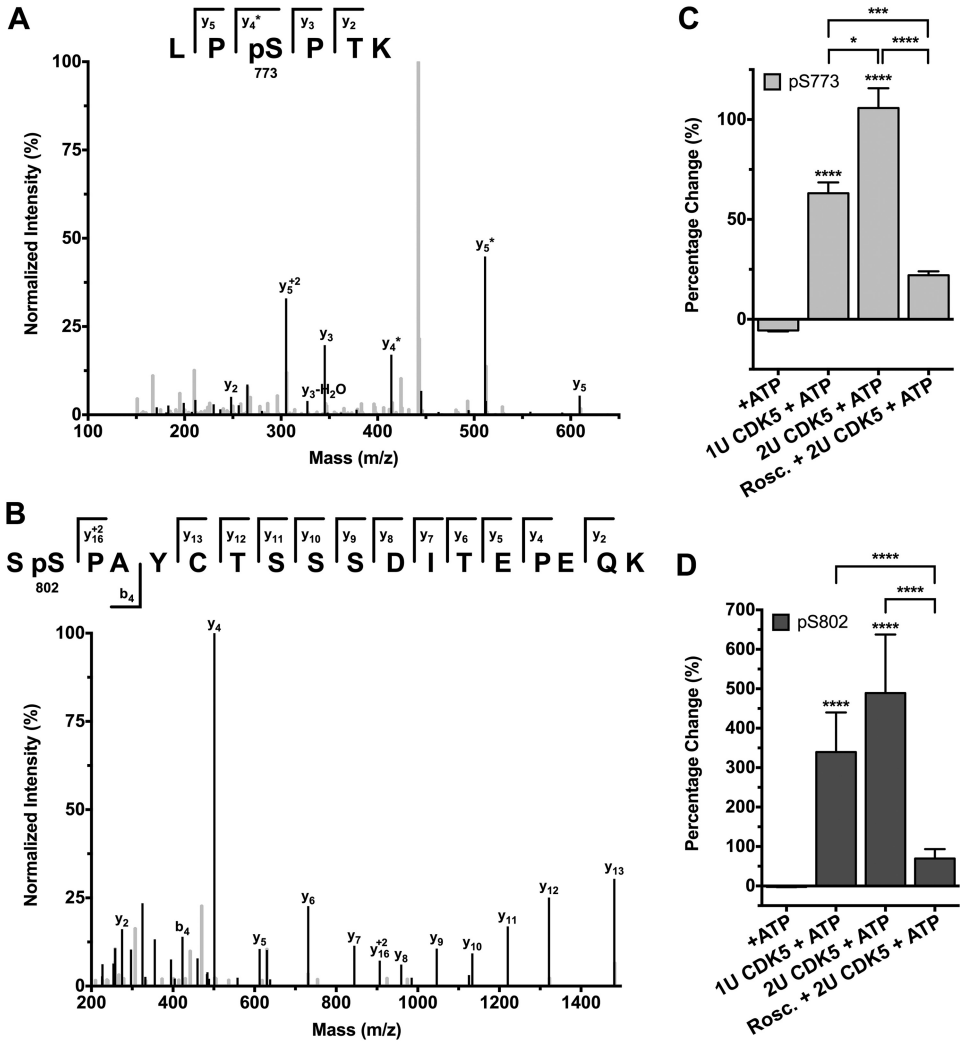

FIGURE 8. **Detection of phosphorylation of synGAP in the PSD fraction at Ser-773 and Ser-802 by mass spectrometry.** *A,* mouse PSD fraction was analyzed with no treatment or after phosphorylation for 10 min in the absence and presence of exogenous CDK5/p35 and roscovitine as described under "Experimental Procedures." Tryptic peptides derived from phosphorylated Ser-773 and Ser-802 on synGAP were detected and subjected to MS/MS analysis on an Orbitrap Fusion as described under "Experimental Procedures." *A,* tryptic digests of synGAP in the isolated PSD fraction without addition of exogenous ATP or kinases were scanned. An HCD MS/MS spectrum of the phosphorylated peptide ^{771}LP(pS)PTK^{776} (doubly charged precursor ion with *m/z* 361.6779) displays a series of y and y* ions (y ion with a neutral loss of phosphoric acid) indicating that Ser-773 is phosphorylated in the PSD fraction. The peaks for *m/z* 150–650 are plotted as relative intensity of peak at *m/z* 442.2288. *B,* HCD MS/MS spectrum of the phosphorylated peptide ^{801}S(pS)PAYCTSSSDITEPEQK^{818} (doubly charged precursor ion with *m/z* 1033.9166), from the same PSD sample as in *A*, displays a series of b and y ions indicating that Ser-802 is phosphorylated. The peaks for *m/z* 200–1485 are plotted as relative intensity of peak at *m/z* 501.2652. *C* and *D,* quantification of synGAP phosphorylation at residues Ser-773 and Ser-802 (*D*) was performed on tryptic peptides from the indicated reactions as described under "Experimental Procedures." Amounts are represented as a percentage change relative to the PSD sample before exposure to exogenous Mg^{2+}/ATP or kinases. Statistical significance was calculated using MSstats utilizing the Benjamini and Hochberg method to produce corrected *p* values. *, $p < 0.05$; ***, $p < 0.001$; ****, $p < 0.0001$. *Rosc,* roscovitine.

serine residues within a CDK5 consensus sequence to study phosphorylation of synGAP by CDK5 in living neurons. We found that it binds to a band of the size of synGAP on immunoblots of proteins from the PSD fraction and to r-synGAP after phosphorylation by purified CDK5 (Fig. 9*A*). We also verified that the antibody binds to synGAP after its immunoprecipitation from a brain membrane fraction with an anti-synGAP antibody, as described under "Experimental Procedures" (Fig. 9*B*). The antibody was raised against an antigen matching the consensus sequence SP*X*(R/K). It binds to phosphorylated mutant synGAPs containing T775A or S802A, but it does not bind to a phosphorylated mutant containing both S773A and T775A, in which Ser-802 is available for phosphorylation (Fig. 9*A*). These data indicate that the antibody recognizes only phosphorylated site Ser-773, which contains a lysine at position +3 in addition to proline at +1. Ser-802 has a proline at +1, but it does not have a basic residue at +3. We were unable to find a commercial antibody that recognizes phosphorylated Ser-802.

Activation of NMDA receptors on cultured neurons allows influx of Ca^{2+} and activation of CaMKII. It has also been shown previously to cause a transient activation of CDK5, followed by down-regulation through degradation of the CDK5 activator p35 (38). Furthermore, prolonged NMDAR activation activates calpain, an activator of CDK5 (39, 40). Calcium influx through NMDA receptors also activates Ras via the guanine nucleotide exchange factor, RasGRF1, and can activate Rap1, possibly via activation of Epac2 or CalDAGGEF1 (9, 41–45). Thus, it is plausible that the relative levels of phosphorylation of synGAP

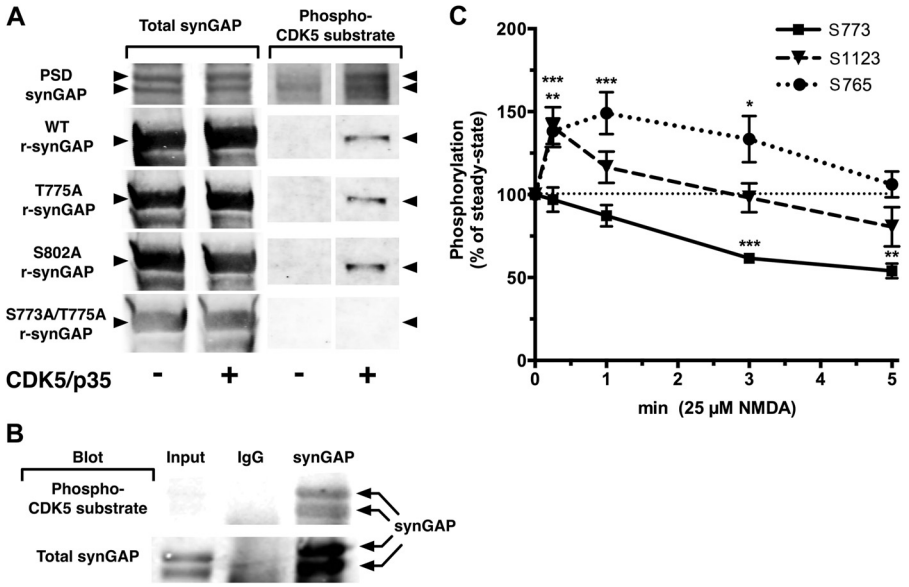

FIGURE 9. **Changes in phosphorylation of synGAP at Ser-773, Ser-765, and Ser-1123 following activation of NMDA receptors in cultured primary neurons.** *A,* commercial anti-CDK5 substrate antibody binds to bands corresponding to synGAP on immunoblots of the PSD fraction and to purified WT and mutant (T775A and S802A) r-synGAP variants phosphorylated with CDK5/p35. The antibody does not bind to a phosphorylated mutant in which Ser-773 is mutated to alanine. *B,* commercial antibody recognizes synGAP after it is immunoprecipitated from a brain membrane fraction with an anti-synGAP antibody as described under "Experimental Procedures." In this experiment, anti-PSD-95 Ab was used as a positive control because synGAP binds to PSD-95. Anti-GluR2 Ab was used as a negative control to show that the immunoprecipitation was specific. PSD-95 was present in the immunoprecipitate and GluR2 was not, as expected (data not shown). *C,* cultured cortical neurons were treated with 25 μM NMDA for 0.25, 1, 3, or 5 min. Phosphorylation of synGAP at Ser-765, Ser-773, and Ser-1123 was measured by immunoblot as described under "Experimental Procedures." *Dotted line,* Ser-765, $n = 9–11$ independent experiments; *Dashed line,* Ser-1123, $n = 9–11$ independent experiments; *solid line,* Ser-773, $n = 5–7$ independent experiments. Levels of phosphoproteins were normalized to intensities of staining for MAP-2. Significance was determined by one sample *t* test compared with 100%. *, $p < 0.05$; **, $p < 0.01$; ***, $p < 0.001$.

by CDK5 and CaMKII, regulated by NMDAR activity, might have an important role in controlling the absolute level, ratio, and duration of NMDAR-dependent Ras and Rap activities at the synapse.

To investigate whether NMDAR activity can regulate phosphorylation of synGAP by CDK5, we measured the time course of phosphorylation of Ser-773 following treatment of cultured cortical neurons with 25 μM NMDA for 15 s to 5 min. For comparison, we also measured phosphorylation of the CaMKII sites, Ser-765 and Ser-1123 (11). Their levels of phosphorylation were measured by immunoblotting neuronal extracts with phospho-site-specific antibodies (11). We detected steady-state phosphorylation of CDK5 sites and of the CaMKII sites in neuronal cultures that were not treated with NMDA. After treatment with 25 μM NMDA, phosphorylation of Ser-765 was elevated at 15 s and peaked at ~1 min, and it returned to baseline at 5 min after addition of NMDA (Fig. 9*C*). As we showed previously (9), phosphorylation at Ser-1123 following treatment with NMDA was biphasic, increasing at 15 s, falling below baseline after a 5-min treatment (Fig. 9*C*), and further below baseline by 10 min (data not shown). In contrast, phosphorylation of the CDK5 site Ser-773 decreased steadily following NMDAR activation (Fig. 9*C*). Thus, the three sites have distinct patterns of regulation during NMDAR activation.

Calcineurin and Protein Phosphatase 2A Differentially Regulate Dephosphorylation of synGAP—To dissect the factors influencing the dynamic phosphorylation patterns of the three sites, we determined which phosphatase activities regulate their phosphorylation at steady state and after NMDAR activation. We tested for involvement of three well known phosphatases, protein phosphatase 1 (PP1), protein phosphatase 2A (PP2A), and calcineurin (CaN). We used cyclosporin A (CsA, 5 μM) as a highly specific inhibitor of CaN and okadaic acid (OKA, 1 μM) to inhibit both PP1 and PP2A. At the extracellular concentration that we used (1 μM), OKA is a more potent inhibitor of PP2A (30). Finally, we used 0.5 μM tautomycin, a PP1-specific inhibitor, to differentiate between the actions of PP1 and PP2A. Tautomycin had little effect on any of the sites (data not shown); therefore, it is likely that most of the effects of OKA resulted from inhibition of PP2A. The inhibitors were applied to cultured cortical neurons for 30 min followed by application of 25 μM NMDA for 0, 0.25, 1, 3, or 5 min. We measured phosphorylation of each of the sites in cortical extracts as described under "Experimental Procedures."

Treatment of cortical cultures with 1 μM OKA resulted in an increase in phosphorylation of Ser-765 at steady state and during the NMDA treatment, indicating that PP2A is involved in maintaining the steady-state level of phosphorylation of Ser-765 under our conditions (Fig. 10*A*). In contrast, 5 μM CsA had no effect on its phosphorylation either at steady state or transiently following NMDA treatment, indicating that CaN does not regulate Ser-765.

Treatment with 1 μM OKA, had a small effect on phosphorylation of Ser-1123 at early times after treatment with NMDA (0.25 and 1 min) but no significant effect at steady state or at later time points (5 min) (Fig. 10*B*). In contrast, treatment with 5 μM CsA increased phosphorylation of Ser-1123 at steady state and also after NMDAR activation with the highest increases occurring at the longer times. The data suggest that, in the absence of inhibitors, NMDA treatment activates CaMKII,

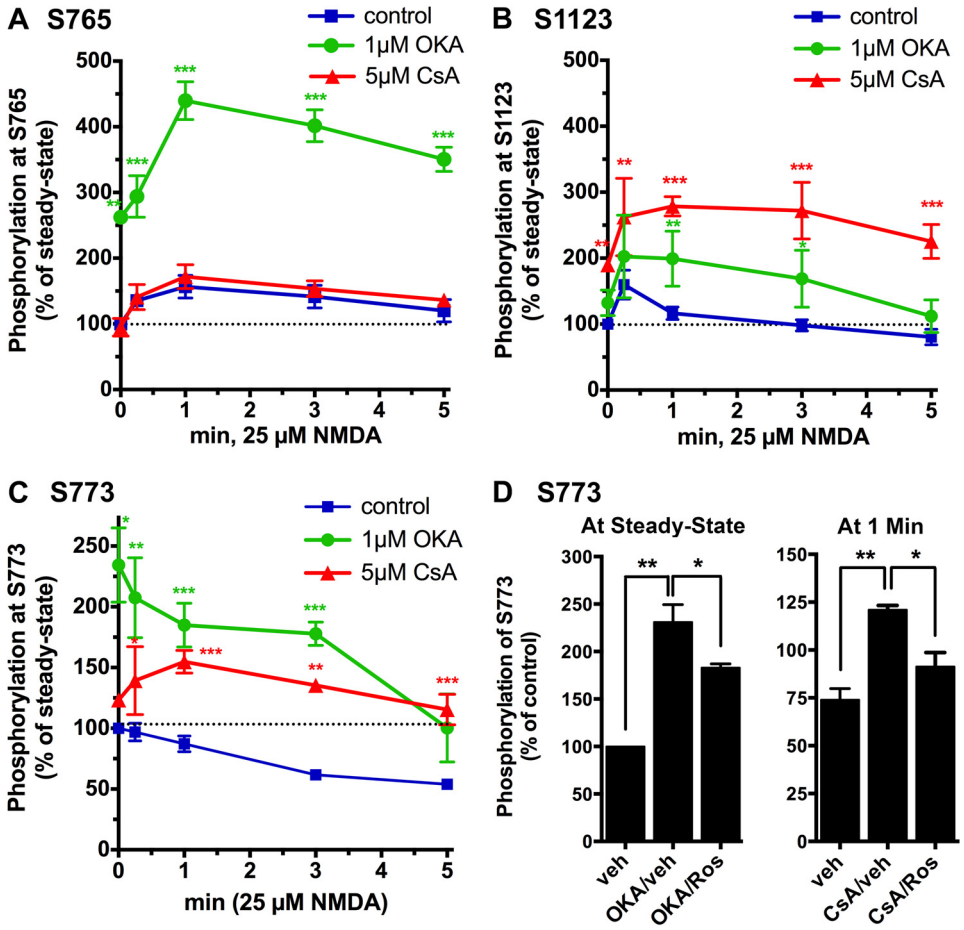

FIGURE 10. **Differential regulation of Ser-773, Ser-765, and Ser-1123 by kinases and phosphatases following activation of NMDA receptors in cultured primary neurons.** To inhibit PP2A or CaN, either okadaic acid (*green*, OKA, 1 μM) or cyclosporin A (*red*, CsA, 5 μM), respectively, were applied to cortical cultures 30 min before addition of 25 μM NMDA for 0.25, 1, 3, or 5 min, as described under "Experimental Procedures." Control cultures (*blue*) were treated as in Fig. 9*C*. Phosphorylation of synGAP at specific sites was measured by immunoblotting as described in Fig. 9*C*. We verified that the effects of OKA in this experiment were a result of inhibition of PP2A by performing complementary experiments with the PP1-specific inhibitor tautomycin, which had very little effect (data not shown). *A,* phosphorylation at Ser-765 was significantly increased at all time points (including steady state) in OKA-treated cultures compared with controls in which no inhibitor was added. In contrast, treatment with CsA had no significant effect on phosphorylation at Ser-765. *B,* phosphorylation at Ser-1123 was significantly increased at 1 and 3 min in OKA-treated cultures, and at all time points in CsA-treated cultures, compared with controls. *C,* phosphorylation of Ser-773 was increased at all time points in the presence of CsA, peaking at 1 min; treatment with OKA increased phosphorylation at steady state and from 15 s to 3 min after NMDA treatment, compared with control. Significance in *A–C* was determined by *t* test, $n = 3–5$ independent experiments. *D, left,* steady-state level of phosphorylation of Ser-773 in cortical cultures is regulated, in part, by CDK5 and PP2A. Cortical cultures were treated with 1 μM OKA for 30 min in the absence or presence of 30 μM roscovitine, which was added 5 min before OKA to block CDK5 prior to inhibition of PP2A. OKA alone increased the steady-state level of phosphorylation of Ser-773 ~2.3-fold. Addition of roscovitine resulted in a significantly smaller increase, supporting the conclusion that CDK5 phosphorylates Ser-773 in neurons independently of treatment with NMDA (OKA/vehicle (*veh*): 231 ± 18%, OKA/roscovitine (*Ros*): 183 ± 4%). Pretreatment with 100 μM roscovitine for 30 min did not further decrease the phosphorylation of Ser-773 (data not shown). Significance was determined by one-sample *t* test compared with 100% and by *t* test, $n = 3–5$ independent experiments. *Right,* transient change in phosphorylation of Ser-773 during activation of NMDA receptors is regulated by CDK5 and CaN. Cortical cultures were treated with NMDA in the absence or presence of 5 μM CsA for 30 min and in the absence or presence of 100 μM roscovitine, which was added 30 min before CsA to block CDK5 prior to inhibition of CaN. Addition of NMDA decreased phosphorylation of Ser-773 to 75% of control in the absence of CsA or roscovitine. The presence of CsA during the treatment with NMDA increased phosphorylation of Ser-773 ~1.5-fold. This effect of CsA was almost completely blocked by simultaneous treatment with roscovitine. Vehicle, 74 ± 6%; CsA/vehicle, 121 ± 2%; CsA/roscovitine, 92 ± 7%. Significance was determined by ANOVA with post hoc Tukey-Kramer multiple comparisons test, $n = 3$ independent experiments. *, $p < 0.05$; **, $p < 0.01$; ***, $p < 0.001$.

leading to rapid phosphorylation of Ser-1123, and it also activates CaN, leading to slower dephosphorylation of Ser-1123. The result is a peak of phosphorylation at 15 s, followed by a gradual fall to below baseline at 5 min. Thus, in contrast to Ser-765, CaN appears to be the primary phosphatase regulating dephosphorylation of Ser-1123.

In contrast to the CaMKII sites, phosphorylation of the CDK5 site Ser-773 slowly decreased during treatment with 25 μM NMDA (Fig. 10*C*), suggesting that phosphatases play a role in NMDA receptor-dependent regulation of this site. Indeed, inhibition of CaN with 5 μM CsA changed the response to a small but significant increase in phosphorylation of Ser-773 at all times other than steady state. These results mean that activation of CaN during treatment with NMDA is responsible for the gradual dephosphorylation of synGAP at Ser-773. It has previously been shown that NMDA treatment can transiently (within 1 min) activate CDK5 activity in cultured neurons (24). Such an increase can only be seen in our data after 1 min of NMDA treatment in the presence of CsA (Fig. 10*C*). Treatment with 1 μM OKA also caused an increase in phosphorylation at Ser-773 at steady state and at early time points, indicating that PP2A dephosphorylates Ser-773 at steady state.

To confirm involvement of CDK5 in the dynamic regulation of phosphorylation of Ser-773, we performed similar experiments in which we incubated neurons with OKA or with OKA and roscovitine, a specific inhibitor of CDK5 (46). The increase in steady-state phosphorylation of Ser-773 in OKA was significantly reduced, although not back to control levels, by pretreatment with 30 μM roscovitine (Fig. 10*D*), verifying that at least a portion of phosphorylation of Ser-773 at steady state is due to CDK5 activity. Pretreatment with a higher concentration of roscovitine (100 μM) did not further decrease the phosphorylation (data not shown), suggesting that another kinase (such as GSK3β) may also phosphorylate Ser-773 in neurons. We also confirmed the involvement of CDK5 in the increased phosphorylation of Ser-773 at 1 min after activation of NMDA receptors in the presence of CsA (Fig. 10*C*). We treated neurons with 5 μM CsA alone or with CsA plus 100 μM roscovitine for 30 min and then applied 25 μM NMDA for 1 min. The increase in phosphorylation of Ser-773 in the presence of CsA is significantly reduced by pretreatment with 100 μM roscovitine (Fig. 10*D*). This result means that phosphorylation of Ser-773 by CDK5 is stimulated by activation of NMDA receptors, and CDK5 accounts for most of the increase in phosphorylation of Ser-773 observed when CaN is inhibited.

DISCUSSION

Biological Role of synGAP—Mutations in synGAP1 are a major cause of nonsyndromic cognitive disability in humans and are particularly common (8–10%) in patients with associated epilepsy or autism (8, 47, 48). Most of the pathogenic mutations characterized to date cause haploinsufficiency. In mice, heterozygous deletion of synGAP, which produces haploinsufficiency, leads to precocious spine formation during development (49, 50), disruption of synaptic plasticity and learning (7, 9), and an increased level of surface AMPA receptors in neurons (51). The deleterious effects of loss of just one copy of synGAP suggest that its functions are rate-limiting for processes that are essential for normal synaptic function.

synGAP accelerates inactivation of the small GTPases Ras and Rap (1, 2, 5, 6). These two GTPases are central regulators in dendrites; in particular, they contribute to regulation of exocytosis and endocytosis of AMPA receptors near the synapse (10). A prolonged increase in active Ras in neurons leads to increased AMPAR exocytosis and thus to an increase in total surface AMPA receptors, whereas prolonged activation of Rap causes an increase in AMPAR endocytosis and a decrease in surface AMPA receptors. The steady-state levels of activity of the two GTPases are set by the balance of production of the active forms by exchange of GDP for GTP and inactivation by GTP hydrolysis. Unphosphorylated synGAP catalyzes inactivation of Rap much more potently than inactivation of Ras (Fig. 2) (6). Thus, its presence would be expected to reduce endocytosis of AMPA receptors relative to their exocytosis by decreasing the steady-state level of active Rap to a greater extent than the steady-state level of active Ras.

Physiological Role of Changes in the Relative Levels of Ras and Rap GAP Activity of synGAP—Here, we have shown that phosphorylation of synGAP by CaMKII increases its ratio of Rap1 GAP to HRas GAP activities. We predict that, in neurons, this would shift the steady-state balance of AMPAR trafficking near the synapse toward exocytosis by decreasing the level of active Rap1 more than active HRas. The net result would be an increase in surface AMPA receptors. Conversely, phosphorylation of r-synGAP by CDK5 decreases its ratio of Rap1 GAP to HRas GAP activities. We predict that this would shift the balance of trafficking near the synapse toward endocytosis of AMPA receptors and lead to a decrease in the number of surface AMPA receptors. Thus, phosphorylation of synGAP could act like a rheostat to create transient changes in the number of surface AMPA receptors or to gradually adjust their steady-state level.

Although r-synGAP increases Rap2 GAP activity, this activity is not altered by any of the phosphorylation events reported here. Both Rap1 and Rap2 are found in pyramidal neurons in the hippocampus and cortex (Allen Mouse Brain Atlas); but, the differences in their functions are not yet clear. There is a precedent for differential regulation of the two forms of Rap. It has been reported that the rasGEF family of proteins catalyze nucleotide exchange for Rap2 but not for Rap1 (52).

Potential Role of Phosphorylation by CaMKII—CaMKII is concentrated in spines and in the PSD (53). It is an early target of Ca^{2+}/calmodulin that is formed in the spine when Ca^{2+} flows through NMDA receptors (45). Active CaMKII phosphorylates Ser-1123 on synGAP at a rapid rate, nearly maximally after 2 min in our assay (Fig. 3*C*). The increase in Rap1 GAP activity of synGAP is also maximal after 2 min of phosphorylation (Fig. 4*E*), suggesting that it is produced by phosphorylation of Ser-1123 or of another rapidly phosphorylated site. We predict that this rapid increase in Rap1 GAP activity would cause a rapid decrease in active Rap1, leading to a relatively rapid decrease in AMPAR endocytosis. The result would be an increase in surface AMPA receptors.

In neurons, we have shown that activation of NMDA receptors produces a rapid increase in phosphorylation of Ser-1123, followed by a slower decrease in phosphorylation mediated by the Ca^{2+}/calmodulin-dependent phosphatase, CaN (Figs. 9*C* and 10*B*). Thus, we predict that the level of active Rap1 would be decreased transiently relative to active HRas, producing a transient increase in the rate of exocytosis of AMPA receptors near the synapse. This rate would decrease gradually as CaN dephosphorylates Ser-1123 and brings the rate of inactivation of Rap1 back down.

It is well established that activation of CaMKII in the spine triggers an increase in synaptic strength produced by enhanced trapping of surface AMPA receptors at the postsynaptic site (45, 54). A slightly slower increase in insertion of surface AMPA receptors near the synapse has been observed after induction of long term potentiation (55). We suggest that phosphorylation of synGAP by CaMKII helps to mediate this transient increase in AMPAR exocytosis.

Potential Role of Phosphorylation by CDK5—In contrast to CaMKII, CDK5 activity is not regulated directly by Ca^{2+} influx or by synaptic activity. Instead, its catalytic subunit is activated by binding to either of two small subunits termed p35 and p39 (14). The p35 and p39 subunits are degraded constitutively; thus, the cellular level of CDK5 activity is maintained by synthesis of the catalytic and regulatory subunits, which are

induced by growth factors, including NGF and BDNF (14). CDK5 is essential for normal brain development and function, but its regulatory roles are generally homeostatic, in contrast to the many transient and activity-dependent regulatory roles of CaMKII (56).

The rate of phosphorylation of synGAP by CDK5 is considerably slower than the rate of phosphorylation by CaMKII (Fig. 3, *A* and *B*). A relatively slow catalytic rate has also been observed for CDK5 with other important neuronal substrates (16). The absence of rapid activation mechanisms and its relatively slow catalytic rate are consistent with a homeostatic role. We postulate that phosphorylation of synGAP by CDK5 may contribute to the homeostatic down-regulation of surface AMPA receptors termed synaptic scaling (57). The mechanisms that contribute to synaptic scaling are complex. Several mechanisms act in parallel to tightly couple the rate of neuronal activity to the total level of surface synaptic AMPA receptors in neurons (57). CDK5 and polo-like kinase 2 (PLK2) have been shown to be necessary for homeostatic reduction of surface AMPA receptors following elevated neuronal activity (58). The two kinases act in concert to phosphorylate spine-associated Rap-specific GAP protein (SPAR), a constitutive synaptic Rap GAP, and tag it for degradation. Loss of SPAR activity increases the steady-state level of active Rap, thus increasing endocytosis of surface AMPA receptors. Our results suggest that CDK5 phosphorylation can also decrease the level of surface AMPA receptors by selectively increasing the Ras GAP activity of synGAP, leading to a reduction of AMPAR exocytosis.

Regulation of synGAP by CDK5 appears to be more complex than its regulation by CaMKII. We have found that two sites on synGAP, Ser-773 and Ser-802, are phosphorylated in isolated PSDs and are phosphorylated concurrently when exogenous CDK5 is added to PSDs (Fig. 8). However, mutations of these two sites suggest that the functional effects of their phosphorylation are quite different (Figs. 6 and 7). Mutations of Ser-773 to alanine (phospho-deficient) or to aspartic acid (phosphomimetic) inhibit HRas GAP and Rap2 GAP activities substantially, and Rap1 GAP activity slightly. This finding means that Ser-773 is crucial for GAP activity itself. In contrast, mutation of Ser-802 to alanine has no effect on GAP activity, although mutation to aspartic acid increases all GAP activities and overrides the effects of mutation of Ser-773. It is interesting that these two sites are located on opposite sides of a 6-residue polyproline motif (Fig. 1*C*) that can form a relatively stiff rod along the protein backbone. It is possible that residues on either side of the polyproline motif play an important role in positioning the downstream portion of the predicted disordered domain with respect to the catalytic domains of synGAP.

We identified a phospho-specific antibody that allowed us to monitor phosphorylation of Ser-773 in cultured neurons; unfortunately, we were unable to monitor phosphorylation of Ser-802. We found that activation of NMDA receptors in cultured neurons triggers slow dephosphorylation of Ser-773 mediated by CaN (Figs. 9*C* and 10*C*). If Ser-802 is also dephosphorylated by CaN, this would reduce HRas GAP activity and help to shift the balance of Ras and Rap activity in favor of active Ras, consistent with our rheostat hypothesis. However, confirmation of the role of Ser-802 will await new reagents or methods.

The large number of serine and threonine phosphorylation sites that we identified for CDK5 (at least 5) and CaMKII (at least 10) are located in clusters within the predicted disordered domain of synGAP (see Fig. 1*C*). This finding is consistent with the proposal of Holt *et al.* and Collins (59, 60) that regulation of protein function by serine/threonine phosphorylation often depends on relatively nonspecific mechanisms that alter protein-protein interactions. These authors found that phosphorylation sites in yeast proteins regulated by CDK1 are often located in clusters that shift position in rapidly evolving disordered domains. We have focused on the functions of two sites phosphorylated by CDK5 (Ser-773 and Ser-802) that are located next to proline residues. However, it is possible, perhaps even likely, that the other three sites can also influence regulatory interactions of the disordered domain with the Ras GAP domain. This possibility is supported by the finding shown in Fig. 7*A* that phosphorylation of sites Ser-728 and Ser-842 can contribute to an increase in HRas GAP activity in addition to phosphorylation of Ser-802.

Significance of Differential Patterns of in Vivo Regulation of Phosphorylation Sites on synGAP—The distinct patterns of regulation of the three phosphorylation sites, Ser-765, Ser-802, and Ser-1123, during synchronous activation of NMDA receptors is striking (Fig. 9*C*). The patterns arise from differential regulation of each site by phosphatases and by kinases (Fig. 10). This precise regulation lends credence to the importance of synGAP in mediating activity-dependent and homeostatic synaptic plasticity.

In summary, phosphorylation of r-synGAP by CaMKII and CDK5 has opposite effects on the ratio of Rap1 GAP and HRas GAP activities of synGAP. We postulate that phosphorylation of synGAP by these two kinases contributes to regulation of the number of surface AMPA receptors in and near spines during synaptic potentiation (CaMKII) and during synaptic scaling (CDK5).

Acknowledgments—We thank Dr. Jost Vielmetter and Michael Anaya of the Beckman Institute Protein Expression Center, Dr. Jie Zhou of the Protein/Peptide Microanalytical Laboratory, and Leslie Schenker of the Kennedy laboratory for technical assistance. The Proteome Exploration Laboratory is supported by the Gordon and Betty Moore Foundation through grant GBMF775 and the Beckman Institute.

REFERENCES

1. Chen, H.-J., Rojas-Soto, M., Oguni, A., and Kennedy, M. B. (1998) A synaptic Ras-GTPase activating protein (p135 SynGAP) inhibited by CaM kinase II. *Neuron* **20,** 895–904
2. Kim, J. H., Liao, D., Lau, L.-F., and Huganir, R. L. (1998) SynGAP: a synaptic RasGAP that associates with the PSD-95/SAP90 protein family. *Neuron* **20,** 683–691
3. Kennedy, M. B., Beale, H. C., Carlisle, H. J., and Washburn, L. R. (2005) Integration of biochemical signalling in spines. *Nat. Rev. Neurosci.* **6,** 423–434
4. Scheffzek, K., Lautwein, A., Kabsch, W., Ahmadian, M. R., and Wittinghofer, A. (1996) Crystal structure of the GTPase-activating domain of human p120GAP and implications for the interaction with Ras. *Nature*

384, 591–596
5. Krapivinsky, G., Medina, I., Krapivinsky, L., Gapon, S., and Clapham, D. E. (2004) SynGAP-MUPP1-CaMKII synaptic complexes regulate p38 MAP kinase activity and NMDA receptor-dependent synaptic AMPA receptor potentiation. *Neuron* **43,** 563–574
6. Pena, V., Hothorn, M., Eberth, A., Kaschau, N., Parret, A., Gremer, L., Bonneau, F., Ahmadian, M. R., and Scheffzek, K. (2008) The C2 domain of SynGAP is essential for stimulation of the Rap GTPase reaction. *EMBO Rep.* **9,** 350–355
7. Komiyama, N. H., Watabe, A. M., Carlisle, H. J., Porter, K., Charlesworth, P., Monti, J., Strathdee, D. J., O'Carroll, C. M., Martin, S. J., Morris, R. G., O'Dell, T. J., and Grant, S. G. (2002) SynGAP regulates ERK/MAPK signaling, synaptic plasticity, and learning in the complex with postsynaptic density 95 and NMDA receptor. *J. Neurosci.* **22,** 9721–9732
8. Hamdan, F. F., Daoud, H., Piton, A., Gauthier, J., Dobrzeniecka, S., Krebs, M. O., Joober, R., Lacaille, J. C., Nadeau, A., Milunsky, J. M., Wang, Z., Carmant, L., Mottron, L., Beauchamp, M. H., Rouleau, G. A., and Michaud, J. L. (2011) *De novo* SYNGAP1 mutations in nonsyndromic intellectual disability and autism. *Biol. Psychiatry* **69,** 898–901
9. Carlisle, H. J., Manzerra, P., Marcora, E., and Kennedy, M. B. (2008) SynGAP regulates steady-state and activity-dependent phosphorylation of cofilin. *J. Neurosci.* **28,** 13673–13683
10. Zhu, J. J., Qin, Y., Zhao, M., Van Aelst, L., and Malinow, R. (2002) Ras and Rap control AMPA receptor trafficking during synaptic plasticity. *Cell* **110,** 443–455
11. Oh, J. S., Manzerra, P., and Kennedy, M. B. (2004) Regulation of the neuron-specific Ras GTPase activating protein, synGAP, by Ca^{2+}/calmodulin-dependent protein kinase II. *J. Biol. Chem.* **279,** 17980–17988
12. Angelo, M., Plattner, F., and Giese, K. P. (2006) Cyclin-dependent kinase 5 in synaptic plasticity, learning and memory. *J. Neurochem.* **99,** 353–370
13. Fu, Z., Lee, S. H., Simonetta, A., Hansen, J., Sheng, M., and Pak, D. T. (2007) Differential roles of Rap1 and Rap2 small GTPases in neurite retraction and synapse elimination in hippocampal spiny neurons. *J. Neurochem.* **100,** 118–131
14. Dhavan, R., and Tsai, L. H. (2001) A decade of CDK5. *Nat. Rev. Mol. Cell Biol.* **2,** 749–759
15. Brinkmann, T., Daumke, O., Herbrand, U., Kühlmann, D., Stege, P., Ahmadian, M. R., and Wittinghofer, A. (2002) Rap-specific GTPase activating protein follows an alternative mechanism. *J. Biol. Chem.* **277,** 12525–12531
16. Morabito, M. A., Sheng, M., and Tsai, L. H. (2004) Cyclin-dependent kinase 5 phosphorylates the N-terminal domain of the postsynaptic density protein PSD-95 in neurons. *J. Neurosci.* **24,** 865–876
17. Dhavan, R., Greer, P. L., Morabito, M. A., Orlando, L. R., and Tsai, L. H. (2002) The cyclin-dependent kinase 5 activators p35 and p39 interact with the α-subunit of Ca^{2+}/calmodulin-dependent protein kinase II and α-actinin-1 in a calcium-dependent manner. *J. Neurosci.* **22,** 7879–7891
18. Klock, H. E., Koesema, E. J., Knuth, M. W., and Lesley, S. A. (2008) Combining the polymerase incomplete primer extension method for cloning and mutagenesis with microscreening to accelerate structural genomics efforts. *Proteins* **71,** 982–994
19. Klock, H. E., and Lesley, S. A. (2009) The polymerase incomplete primer extension (PIPE) method applied to high-throughput cloning and site-directed mutagenesis. *Methods Mol. Biol.* **498,** 91–103
20. Wang, W., and Malcolm, B. A. (1999) Two-stage PCR protocol allowing introduction of multiple mutations, deletions and insertions using QuikChange site-directed mutagenesis. *BioTechniques* **26,** 680–682
21. Miller, S. G., and Kennedy, M. B. (1985) Distinct forebrain and cerebellar isozymes of type II Ca^{2+}/calmodulin-dependent protein kinase associate differently with the postsynaptic density fraction. *J. Biol. Chem.* **260,** 9039–9046
22. Kupzig, S., Deaconescu, D., Bouyoucef, D., Walker, S. A., Liu, Q., Polte, C. L., Daumke, O., Ishizaki, T., Lockyer, P. J., Wittinghofer, A., and Cullen, P. J. (2006) GAP1 family members constitute bifunctional Ras and Rap GTPase-activating proteins. *J. Biol. Chem.* **281,** 9891–9900
23. Bollag, G., and McCormick, F. (1995) Intrinsic and GTPase-activating protein-stimulated Ras GTPase assays. *Methods Enzymol.* **255,** 161–170
24. Leupold, C. M., Goody, R. S., and Wittinghofer, A. (1983) Stereochemistry of the elongation factor Tu X GTP complex. *Eur. J. Biochem.* **135,** 237–241
25. Kalli, A., and Hess, S. (2012) Effect of mass spectrometric parameters on peptide and protein identification rates for shotgun proteomic experiments on an LTQ-orbitrap mass analyzer. *Proteomics* **12,** 21–31
26. Timm, W., Ozlu, N., Steen, J. J., and Steen, H. (2010) Effect of high-accuracy precursor masses on phosphopeptide identification from MS3 spectra. *Anal. Chem.* **82,** 3977–3980
27. Savitski, M. M., Lemeer, S., Boesche, M., Lang, M., Mathieson, T., Bantscheff, M., and Kuster, B. (2011) Confident phosphorylation site localization using the Mascot Delta Score. *Mol. Cell. Proteomics* **10,** M110.003830
28. Shevchenko, A., Tomas, H., Havlis, J., Olsen, J. V., and Mann, M. (2006) In-gel digestion for mass spectrometric characterization of proteins and proteomes. *Nat. Protoc.* **1,** 2856–2860
29. Peterson, A. C., Russell, J. D., Bailey, D. J., Westphall, M. S., and Coon, J. J. (2012) Parallel reaction monitoring for high resolution and high mass accuracy quantitative, targeted proteomics. *Mol. Cell. Proteomics* **11,** 1475–1488
30. MacLean, B., Tomazela, D. M., Shulman, N., Chambers, M., Finney, G. L., Frewen, B., Kern, R., Tabb, D. L., Liebler, D. C., and MacCoss, M. J. (2010) Skyline: an open source document editor for creating and analyzing targeted proteomics experiments. *Bioinformatics* **26,** 966–968
31. Choi, M., Chang, C. Y., Clough, T., Broudy, D., Killeen, T., MacLean, B., and Vitek, O. (2014) MSstats: an R package for statistical analysis of quantitative mass spectrometry-based proteomic experiments. *Bioinformatics* **30,** 2524–2526
32. Carlisle, H. J., Luong, T. N., Medina-Marino, A., Schenker, L., Khorosheva, E., Indersmitten, T., Gunapala, K. M., Steele, A. D., O'Dell, T. J., Patterson, P. H., and Kennedy, M. B. (2011) Deletion of densin-180 results in abnormal behaviors associated with mental illness and reduces mGluR5 and DISC1 in the postsynaptic density fraction. *J. Neurosci.* **31,** 16194–16207
33. Carlin, R. K., Grab, D. J., Cohen, R. S., and Siekevitz, P. (1980) Isolation and characterization of postsynaptic densities from various brain regions: enrichment of different types of postsynaptic densities. *J. Cell Biol.* **86,** 831–845
34. Brewer, G. J., Torricelli, J. R., Evege, E. K., and Price, P. J. (1993) Optimized survival of hippocampal neurons in B27-supplemented Neurobasal™, a new serum-free medium combination. *J. Neurosci. Res.* **35,** 567–576
35. Fersht, A. (1999) *Structure and Mechanism in Protein Science: A Guide to Enzyme Catalysis and Protein Folding*, pp. 362–368, W. H. Freeman & Co., New York
36. John, J., Schlichting, I., Schiltz, E., Rösch, P., and Wittinghofer, A. (1989) C-terminal truncation of p21H preserves crucial kinetic and structural properties. *J. Biol. Chem.* **264,** 13086–13092
37. Frech, M., John, J., Pizon, V., Chardin, P., Tavitian, A., Clark, R., McCormick, F., and Wittinghofer, A. (1990) Inhibition of GTPase activating protein stimulation of Ras-p21 GTPase by the Krev-1 gene product. *Science* **249,** 169–171
38. Wei, F. Y., Tomizawa, K., Ohshima, T., Asada, A., Saito, T., Nguyen, C., Bibb, J. A., Ishiguro, K., Kulkarni, A. B., Pant, H. C., Mikoshiba, K., Matsui, H., and Hisanaga, S. (2005) Control of cyclin-dependent kinase 5 (Cdk5) activity by glutamatergic regulation of p35 stability. *J. Neurochem.* **93,** 502–512
39. Adamec, E., Beermann, M. L., and Nixon, R. A. (1998) Calpain I activation in rat hippocampal neurons in culture is NMDA receptor selective and not essential for excitotoxic cell death. *Brain Res. Mol. Brain Res.* **54,** 35–48
40. Wu, H. Y., Yuen, E. Y., Lu, Y. F., Matsushita, M., Matsui, H., Yan, Z., and Tomizawa, K. (2005) Regulation of *N*-methyl-D-aspartate receptors by calpain in cortical neurons. *J. Biol. Chem.* **280,** 21588–21593
41. Chen, Y., Wang, P. Y., and Ghosh, A. (2005) Regulation of cortical dendrite development by Rap1 signaling. *Mol. Cell. Neurosci.* **28,** 215–228
42. Krapivinsky, G., Krapivinsky, L., Manasian, Y., Ivanov, A., Tyzio, R., Pellegrino, C., Ben-Ari, Y., Clapham, D. E., and Medina, I. (2003) The NMDA receptor is coupled to the ERK pathway by a direct interaction between NR2B and RasGRF1. *Neuron* **40,** 775–784
43. Li, S., Tian, X., Hartley, D. M., and Feig, L. A. (2006) Distinct roles for Ras-guanine nucleotide-releasing factor 1 (Ras-GRF1) and Ras-GRF2 in the induction of long-term potentiation and long-term depression. *J. Neu-*

rosci. **26,** 1721–1729
44. Penzes, P., Woolfrey, K. M., and Srivastava, D. P. (2011) Epac2-mediated dendritic spine remodeling: implications for disease. *Mol. Cell. Neurosci.* **46,** 368–380
45. Kennedy, M. B. (2013) Synaptic signaling in learning and memory. *Cold Spring Harb. Perspect. Biol.* 2013 a016824
46. De Azevedo, W. F., Leclerc, S., Meijer, L., Havlicek, L., Strnad, M., and Kim, S. H. (1997) Inhibition of cyclin-dependent kinases by purine analogues: crystal structure of human cdk2 complexed with roscovitine. *Eur. J. Biochem.* **243,** 518–526
47. Berryer, M. H., Hamdan, F. F., Klitten, L. L., Møller, R. S., Carmant, L., Schwartzentruber, J., Patry, L., Dobrzeniecka, S., Rochefort, D., Neugnot-Cerioli, M., Lacaille, J. C., Niu, Z., Eng, C. M., Yang, Y., Palardy, S., Belhumeur, C., Rouleau, G. A., Tommerup, N., Immken, L., Beauchamp, M. H., Patel, G. S., Majewski, J., Tarnopolsky, M. A., Scheffzek, K., Hjalgrim, H., Michaud, J. L., and Di Cristo, G. (2013) Mutations in SYNGAP1 cause intellectual disability, autism, and a specific form of epilepsy by inducing haploinsufficiency. *Hum. Mutat.* **34,** 385–394
48. Hamdan, F. F., Gauthier, J., Spiegelman, D., Noreau, A., Yang, Y., Pellerin, S., Dobrzeniecka, S., Côté, M., Perreau-Linck, E., Perreault-Linck, E., Carmant, L., D'Anjou, G., Fombonne, E., Addington, A. M., Rapoport, J. L., Delisi, L. E., Krebs, M. O., Mouaffak, F., Joober, R., Mottron, L., Drapeau, P., Marineau, C., Lafrenière, R. G., Lacaille, J. C., Rouleau, G. A., Michaud, J. L., and Synapse to Disease Group. (2009) Mutations in SYNGAP1 in autosomal nonsyndromic mental retardation. *N. Engl. J. Med.* **360,** 599–605
49. Vazquez, L. E., Chen, H. J., Sokolova, I., Knuesel, I., and Kennedy, M. B. (2004) SynGAP regulates spine formation. *J. Neurosci.* **24,** 8862–8872
50. Clement, J. P., Aceti, M., Creson, T. K., Ozkan, E. D., Shi, Y., Reish, N. J., Almonte, A. G., Miller, B. H., Wiltgen, B. J., Miller, C. A., Xu, X., and Rumbaugh, G. (2012) Pathogenic SYNGAP1 mutations impair cognitive development by disrupting maturation of dendritic spine synapses. *Cell* **151,** 709–723
51. Kim, J. H., Lee, H. K., Takamiya, K., and Huganir, R. L. (2003) The role of synaptic GTPase-activating protein in neuronal development and synaptic plasticity. *J. Neurosci.* **23,** 1119–1124
52. Yaman, E., Gasper, R., Koerner, C., Wittinghofer, A., and Tazebay, U. H. (2009) RasGEF1A and RasGEF1B are guanine nucleotide exchange factors that discriminate between Rap GTP-binding proteins and mediate Rap2-specific nucleotide exchange. *FEBS J.* **276,** 4607–4616
53. Kennedy, M. B. (2000) Signal-processing machines at the postsynaptic density. *Science* **290,** 750–754
54. Opazo, P., Labrecque, S., Tigaret, C. M., Frouin, A., Wiseman, P. W., De Koninck, P., and Choquet, D. (2010) CaMKII triggers the diffusional trapping of surface AMPARs through phosphorylation of stargazin. *Neuron* **67,** 239–252
55. Makino, H., and Malinow, R. (2009) AMPA receptor incorporation into synapses during LTP: the role of lateral movement and exocytosis. *Neuron* **64,** 381–390
56. Su, S. C., and Tsai, L. H. (2011) Cyclin-dependent kinases in brain development and disease. *Annu. Rev. Cell Dev. Biol.* **27,** 465–491
57. Turrigiano, G. (2012) Homeostatic synaptic plasticity: local and global mechanisms for stabilizing neuronal function. *Cold Spring Harb. Perspect. Biol.* **4,** a005736
58. Seeburg, D. P., Feliu-Mojer, M., Gaiottino, J., Pak, D. T., and Sheng, M. (2008) Critical role of CDK5 and Polo-like kinase 2 in homeostatic synaptic plasticity during elevated activity. *Neuron* **58,** 571–583
59. Holt, L. J., Tuch, B. B., Villén, J., Johnson, A. D., Gygi, S. P., and Morgan, D. O. (2009) Global analysis of Cdk1 substrate phosphorylation sites provides insights into evolution. *Science* **325,** 1682–1686
60. Collins, M. O. (2009) Cell biology. Evolving cell signals. *Science* **325,** 1635–1636